GROWTH AND CHARACTERIZATION OF III-V SEMICONDUCTOR MATERIALS FOR MOCVD REACTOR QUALIFICATION AND PROCESS CONTROL

BY

KEVIN PAUL BASSETT

THESIS

Submitted in partial fulfillment of the requirements
for the degree of Master of Science in Electrical and Computer Engineering
in the Graduate College of the
University of Illinois at Urbana-Champaign, 2009

Urbana, Illinois

Adviser:

Assistant Professor Xiuling Li

ABSTRACT

Metalorganic chemical vapor deposition is examined as a technique for growing compound semiconductor structures. Material analysis techniques for characterizing the quality and properties of compound semiconductor material are explained and data from recent commissioning work on a newly installed reactor at the University of Illinois is presented.

To my mother and father for their never ending support, and to my brother for making me believe I could go farther.

ACKNOWLEDGMENTS

The author would like to thank Xiuling Li for the opportunity to work on such a unique and rewarding project.

The author would like to thank Dane Sievers and Rob Hasken for their invaluable support and advice throughout the last two years that undoubtedly contributed to the success of this project. The author would also like to thank Ken Tarman and the MNTL staff for their help and support.

High resolution x-ray diffraction was carried out in the Frederick Seitz Materials Research Laboratory Central Facilities, University of Illinois, which are partially supported by the U.S. Department of Energy under grants DE-FG02-07ER46453 and DE-FG02-07ER46471.

TABLE OF CONTENTS

CHAPTER 1

INTRODUCTION

Metal-organic chemical vapor deposition (MOCVD) is a technique for thin film deposition using metalorganic compounds as source materials. Metalorganic sources are also referred to as organometallics (OM); vapor phase epitaxy (VPE) is also sometimes used instead of CVD, thus leading to many acronym permutations (MOVPE, OMCVD, etc.). All of these names refer to the same technique with the caveat that epitaxy refers to a special case of film deposition where the substrate is crystalline, and the deposited layers continue that crystal structure [1].

There are many applications of MOCVD technology. Metalorganic precursors have been used to deposit thin films of metals for use in the integrated circuit (IC) industry, ferromagnetics for use in the memory industry, and dielectrics via atomic layer deposition. The primary application of MOCVD technology is the growth of compound semiconductor material for electronic devices.

A proper discussion of the MOCVD process would involve analysis of the complex thermodynamics and fluid mechanics involved. Although far beyond the scope of this paper, several good texts have been written on the subject [2], [3].

In this paper, after a brief discussion of the technique of MOCVD, a discussion on the design of AIXTRON AIX 200 series MOCVD reactors will lead into a specific discussion on the commissioning of one such reactor at the University of Illinois Micro and Nanotechnology Lab (MNTL). Analysis techniques used to evaluate the quality and properties of material grown in the reactor will be explained; the results of this analysis will then be presented and compared to established results. Finally, a case study on the growth of semiconductor nanotubes will demonstrate the current performance of the reactor.

CHAPTER 2

MOCVD TECHNIQUE

Precursors for MOCVD must fulfill several key requirements. They must pyrolyze in the range of typical process temperatures, but be stable near room temperature for transport and storage. Solid and liquid precursors must have sufficiently high vapor pressures to be drawn into the reactor in gas phase. Different precursors used in the same process must not react to form byproducts in the gas phase when mixed before injection into the reactor. Finally, precursors must be available in extremely high purity to grow high quality semiconductor material. Ideally such sources would also be non-hazardous and inexpensive. In reality, the materials that best satisfy the process requirements happen to be quite expensive, extremely toxic, and react violently with oxygen and water. However, with special handling procedures, good reactor design, and adequate precautions these materials can be safely utilized. Several good articles on the environmental health and safety aspects of MOCVD have been written [4], [5].

The precursors commonly used in MOCVD fit into two main categories: metalorganics and hydrides.

2.1 Metalorganics

Metalorganics are typically alkyls of metals. Methyl and ethyl radicals are most common, but occasionally more complex molecular structures are required to obtain the required properties discussed above. Some commonly used metalorganics are listed in Table 2.1.

Since most metalorganics are highly toxic and reactive with oxygen, they are contained in stainless steel vessels called bubblers. These containers have an internal dip tube that is used to "bubble" a carrier gas, typically hydrogen, through the liquid or solid source material thus drawing off the

Table 2.1: Commonly used metalorganic precursors and their vapor pressures at 10° C. Vapor pressure data from Akzo Nobel High Purity Metal Organics.

Element	Name	Symbol	Vapor Pressure @ 10° C (torr)
Ga	trimethylgallium	TMGa	113.6
	triethylgallium	TEGa	2.8
Al	trimethylaluminum	TMAl	4.87
	triethylaluminum	TEAl	.005
In	trimethylindium	TMIn	.46
Sb	trimethylantimony	TMSb	52.1
	triethylantimony	TESb	1.56
Zn	dimethylzinc	DMZn	195.2
	diethylzinc	DEZn	6.79
As	tertiarybutylarsenic	TBA	125 @ 20° C[1]
P	tertiarybutylphosphorous	TBP	250 @ 20° C[1]

vapor to be carried to the reactor. Bubblers are kept in temperature controlled baths to keep vapor pressure constant, as it is strongly dependent on temperature. This knowledge of the vapor pressure along with the carrier gas flow into the bubbler is sufficient to calculate the mass transport of the precursor to the reactor [1].

2.2 Hydrides

Hydride precursors such as arsine (AsH_3), phosphine (PH_3) and ammonia (NH_3) are often used in the growth of compound semiconductors because they can be highly purified and are inexpensive compared to their metalorganic equivalents (TBA and TBP). Although the hydride gases are typically much more hazardous than metalorganics, they are still much more commonly used due to their availability at higher purities and lower cost [1]. Silane and disilane are also commonly used hydride precursors for silicon. Some hydride sources are partially or fully halogenated. Two common carbon sources are carbon tetrachloride (CCl_4) and carbon tetrabromide (CBr_4). Chlorinated silanes and disilanes are also common.

2.3 Growth Process

In the MOCVD process, mass transport of precursor molecules into the reaction chamber is precisely controlled with mass flow controllers (MFC) and pressure controllers (PC). In the reaction chamber the precursor molecules are exposed to the material substrate which is located on a susceptor that has been preheated to the desired growth temperature. The heat of the substrate then pyrolyzes the precursors. The radicals and atoms freed by this process may then adsorb onto the crystal surface where they will either get incorporated into the crystal structure as it grows, or desorb from the surface. Complex hydrodynamic and thermodynamic processes govern the growth and stoichiometry of the crystal [2]. The sheer complexity of the MOCVD process has led to a common sentiment that crystal growth is as much an art as a science.

2.4 Reactor Designs

Many different types of MOCVD reactors have been designed and built. These reactors vary in their geometry, operating pressure, and temperature control among other things. Geometrically, most can be split into two basic groups: horizontal and vertical. In a vertical reactor setup, the precursors are introduced perpendicularly to the surface of the substrate. By contrast, in a horizontal reactor the precursors flow parallel to the substrate surface. In order to improve the thickness and composition uniformity of the layers grown, susceptors are rotated. MOCVD reactors typically operate at atmospheric or low pressure (LP-CVD), although high pressure designs also exist [6]. Heating of the substrate is typically accomplished by RF induction heating, infrared heating from halogen lamps, or resistive heating.

CHAPTER 3

AIXTRON AIX 200/4 MOCVD

An AIXTRON AIX 200/4 reactor was donated by Honeywell Inc. to the University of Illinois for use in the Micro and Nanotechnology Lab. Installing the reactor in the cleanroom and commissioning it was a monumental task. The author has spent the last two years rebuilding this system, upgrading the building facilities to support it, and characterizing the material grown.

AIX 200 Series reactors are horizontal flow IR heated LP-MOCVD reactors intended for research or small scale production of compound semiconductors. The 200/4 variant can handle wafers up to four inches in diameter [7].

3.1 Overhaul and Refitting

After decommissioning and crating for shipment at Honeywell, a significant amount time passed before the reactor arrived at MNTL. This period of inactivity combined with some damage sustained during shipment presented many potential performance and safety issues. To ensure the performance and safety of the system, a complete overhaul of the system was performed. Due to the extremely hazardous nature of the tool, this overhaul was done with the utmost scrutiny. During the final helium leak check, every section of plumbing was tested at least twice with a maximum passing leak rate of $1 * 10^{-9}$ $\frac{\text{atm*cc}}{\text{s}}$. The exhaust handling system was nearly completely refit. A new trap system was designed and installed with a particulate filter for arsenic capture and cold trap for phosphorous condensing. The process vacuum pump was professionally rebuilt.

3.2 Facilities Integration

Installation of this reactor required integration with MNTL's existing toxic gas delivery, safety monitoring, and exhaust treatment systems. Existing Semigas toxic gas handling cabinets were refit to handle the pure arsine and phosphine cylinders required for the reactor. Hydrogen and toxic gas monitoring equipment was integrated into the system for safety monitoring. A controlled decomposition and oxidation furnace (CDO) was acquired and installed to safely handle the dangerous exhaust gas stream from the reactor. The CDO's safety interlock was tied into the reactor's safety control system and tested for proper operation.

3.3 System Schematic

AIXTRON system number 1217 was originally designed to accomodate four hydride sources, seven regular metal-organic (MO) sources and one dilution metal-organic source. The mass flow controllers (MFC), pressure controllers (PC), and plumbing for two of the seven regular MO sources and one of the hydride sources were not installed upon initial comissioning of the system. At some point, the original owner, Honeywell Inc., decided to re-fit the system to accomodate four regular MO sources and three dilution MO sources. This allowed two trimethylgallium and two trimethylaluminum sources to be installed in the system, one each on two of the regular MO lines and two of the dilution source lines. Presumably, this was done to allow for faster growth of AlGaAs distributed Bragg reflector (DBR) structures for vertical cavity surface emitting lasers (VCSELs) by eliminating the need to spend time changing and stabilizing MO source flow rates between layers of the DBR.

Figure 3.1 is a schematic of the present plumbing layout of system 1217. This figure was modified from the original in the system manual to reflect the changes to the system. Figure 3.2 depicts the original schematic of the system, unaltered from the system manual.

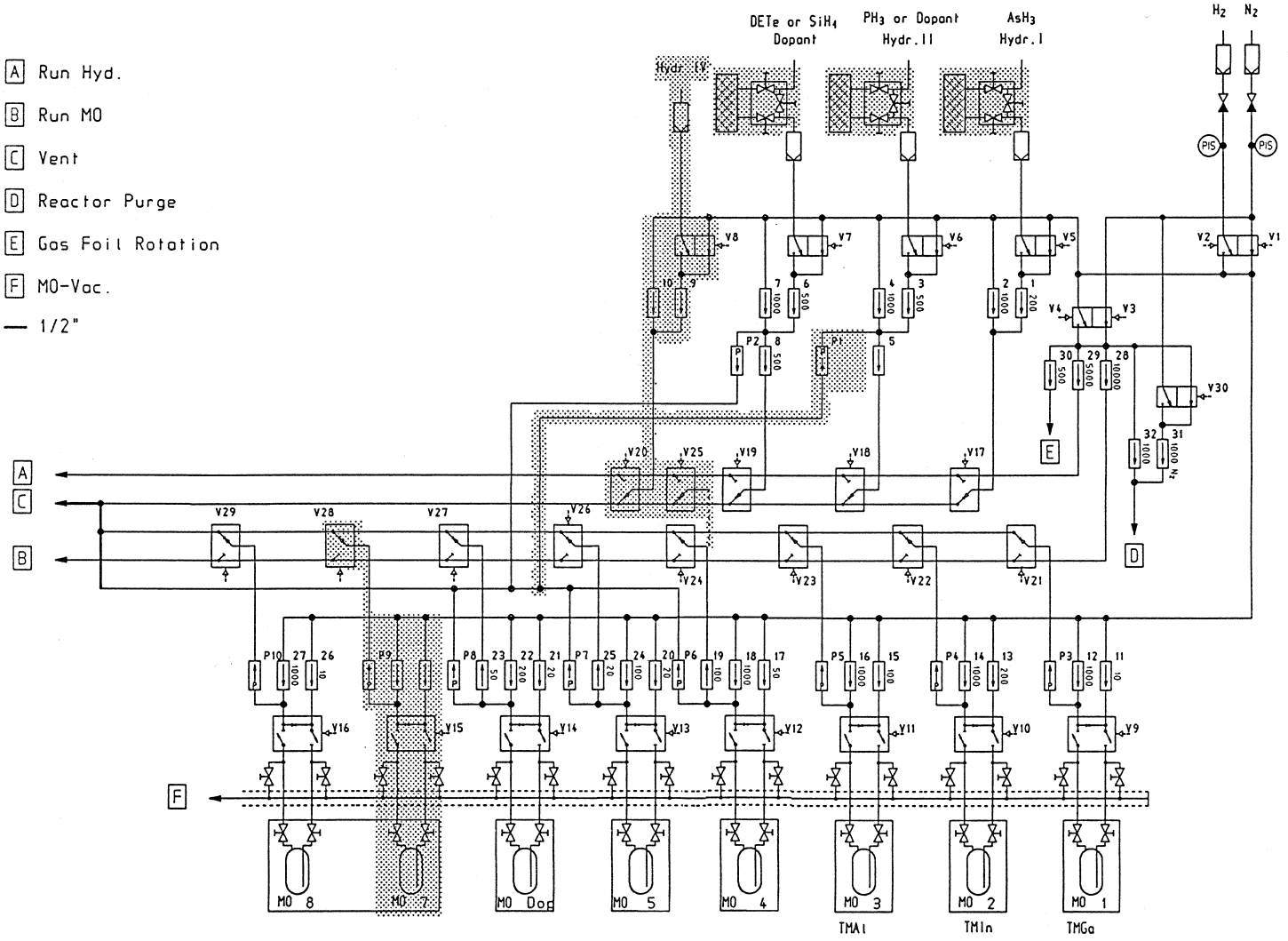

Figure 3.1: Schematic of AIX 200/4 S/N 1217, modified from original to reflect upgrades and changes to the system since initial commissioning [7].

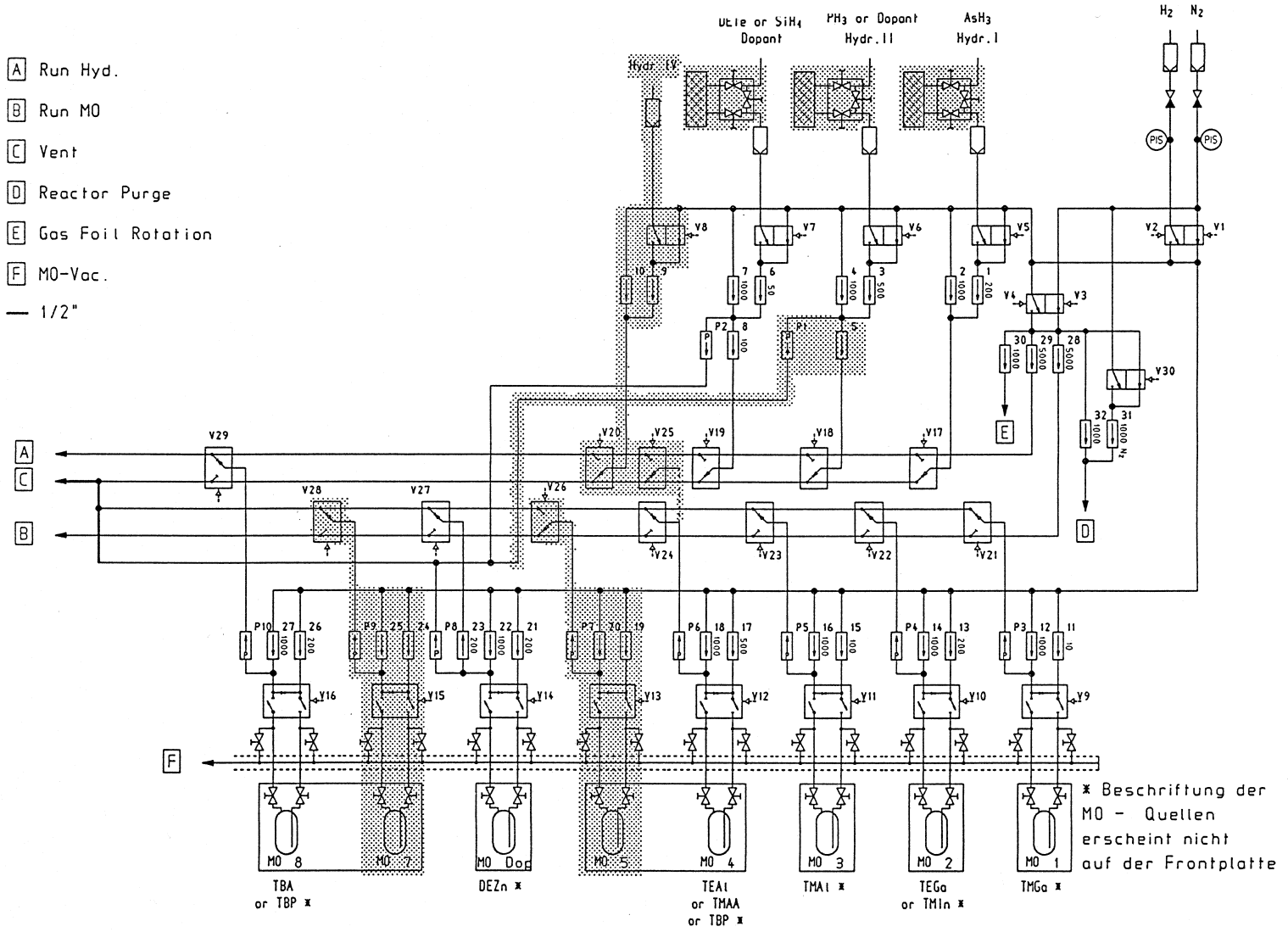

Figure 3.2: Schematic of AIX 200/4 S/N 1217, unaltered from manual, reflecting the configuration of the system on initial comissioning [7].

3.4 CACE

AIXTRON's Computer Aided Control Environment (CACE) software enables computer based automation of AIXTRON MOCVD systems. On startup, it loads an initialization file and a graphical environment setup file that contain information on a specific system's current configuration. The names of these files are derived from the system serial number: in the case of system 1217 the files are named 1217.INI and 1217.GRF respectively [8]. Honeywell Inc. restored the CACE software to its original version before shipping the system to the University of Illinois. The author modified the initialization file and graphical environment setup file to match the current configuration of the reactor so all of the hydride and metalorganic sources would function properly. The initialization file is included in Appendix A; the grapical environment setup file has been omitted due to its non-human-readable format and excessive length.

To perform a computer controlled growth run using CACE, the growth instructions and parameters for the reactor must be specified in a file called a recipe. Recipes are edited in WinEPI and written in a proprietary EPI language that is well documented in the CACE User Manual [8]. A template recipe for system 1217 has been included in Appendix B.

3.5 Reaction Vessel Design

The reaction vessel is characterized by both inner and outer quartz tubes, a load lock mechanism, and a port for an in-situ monitor. The reactor design is illustrated in Figure 3.3.

The outer quartz tube acts as the containment and pressure vessel. The inner quartz tube has several functions: it establishes the complicated flow dynamics in the reactor, holds the susceptor in place on a set of tracks, and simplifies cleaning of the reactor. The inlet of the inner quartz tube connects via a ball joint to the precursor inlet chamber. The MO and hydride sources are injected into two separate channels in the inlet chamber to avoid unwanted gas phase reactions that could precipitate contaminating particles and deplete the stream of reagents. A horizontal laminar flow plate in the inner liner continues to keep these precursor streams separate

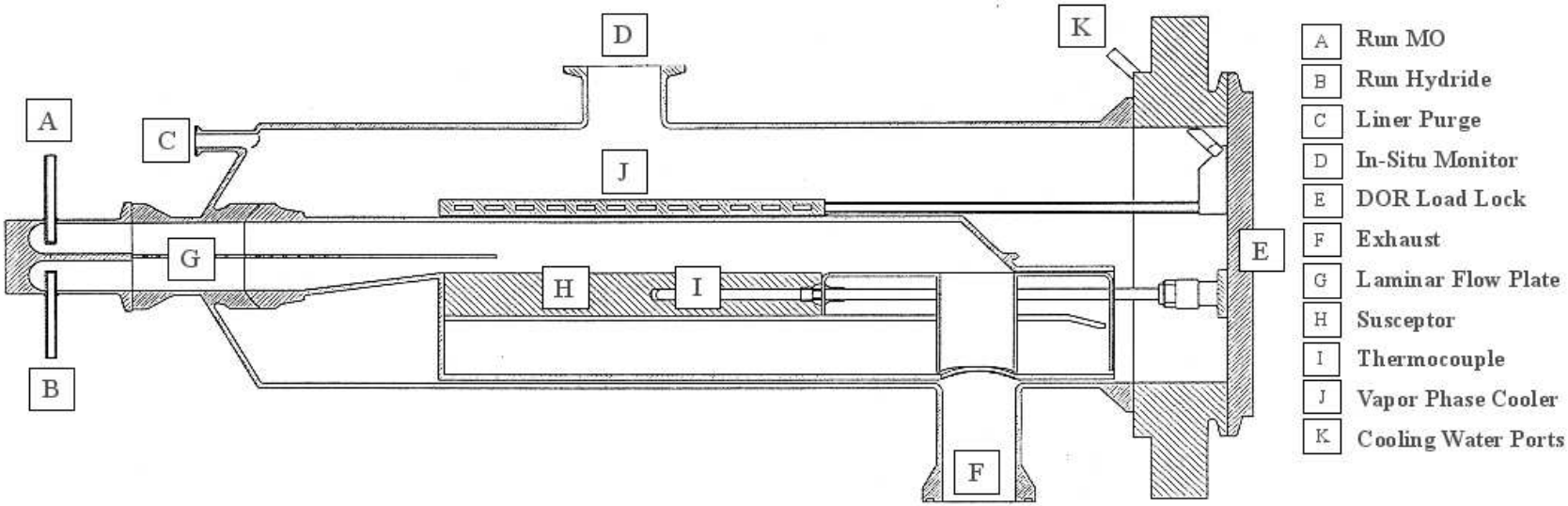

Figure 3.3: Drawing of the quartz reaction vessel of an AIXTRON AIX 200 Series MOCVD reactor. Image modified from original to match the current state of the reactor [7].

until just before interaction with the substrate. The tracks that the susceptor sits on keep it mechanically stable during growth and allow it to slide easily when it is extracted into the glove box for sample loading and unloading. Once the susceptor is pulled into the glove box through the load lock, the entire inner liner tube may also be easily removed. This greatly simplifies the reactor cleaning process as the inner tube may be removed, deposition cleaned off, and replaced without affecting any of the leak tight seals. Thus a time-consuming leak check can be avoided. Deposition on the outer quartz tube during growth is avoided by applying a constant purge of carrier gas to the space between the quartz tubes through the liner purge port.

Positioned above the susceptor on top of the inner quartz tube is a stainless steel cooling plate known as the vapor phase cooler. A hole in the center of the vapor phase cooler allows light to pass through so optical in-situ monitoring equipment can be mounted and focused on the surface of the substrate.

To ensure the load lock door is sealed after being opened and closed, a system known as a double o-ring is employed. The reactor door seals with two concentric o-rings and the space between the o-rings is evacuated before growth. Should even a small leak develop in the door seal, the pressure will rise quickly in the small volume between the o-rings. This pressure is monitored at all times, and if it passes a certain threshold value the system will automatically reset itself to a safe state to prevent toxic gas leakage [7].

CHAPTER 4

CHARACTERIZATION

4.1 Hall Effect

Conduction theory in solids is significantly complicated by the facts that scattering is dependent on momentum, the band structure is important to the equations of motion, and analysis must be done statistically due to the presence of many carriers in the solid. To avoid these complications, Drude proposed a simple model that assumed that every electron moved with velocity $\boldsymbol{v}$ according to equation (4.1) where $\boldsymbol{F}_f$ is a frictional force that represents the action of scattering and is defined as in equation (4.2)[9].

$$m\dot{\boldsymbol{v}} = \boldsymbol{F_0} - \boldsymbol{F}_f \tag{4.1}$$

$$\boldsymbol{F}_f = m\boldsymbol{v}/\tau, \tag{4.2}$$

With this simple model the current density can be calculated in terms of the number of electrons and the velocity at which they move:

$$\boldsymbol{j} = en\boldsymbol{v} \tag{4.3}$$

The band structure can be included by using the effective mass. We can use the Drude theory to examine the special case of the Hall effect in which the force on the electrons is due to an electric field $\boldsymbol{E}$ and a magnetic field $\boldsymbol{B}$.

$$m^*\dot{\boldsymbol{v}} = -e\left(\boldsymbol{E} + \boldsymbol{v} \times \boldsymbol{B}\right) - m\boldsymbol{v}/\tau \tag{4.4}$$

We further specify, as illustrated in Figure 4.1, the magnetic field $\boldsymbol{B} = B_z$ and the electric field $\boldsymbol{E} = E_x + E_y$. As a voltage V_{CD} is applied, current I_x flows but the magnetic field deflects the carriers towards the edge of the sample. As the carriers build up at the edge of the sample, they

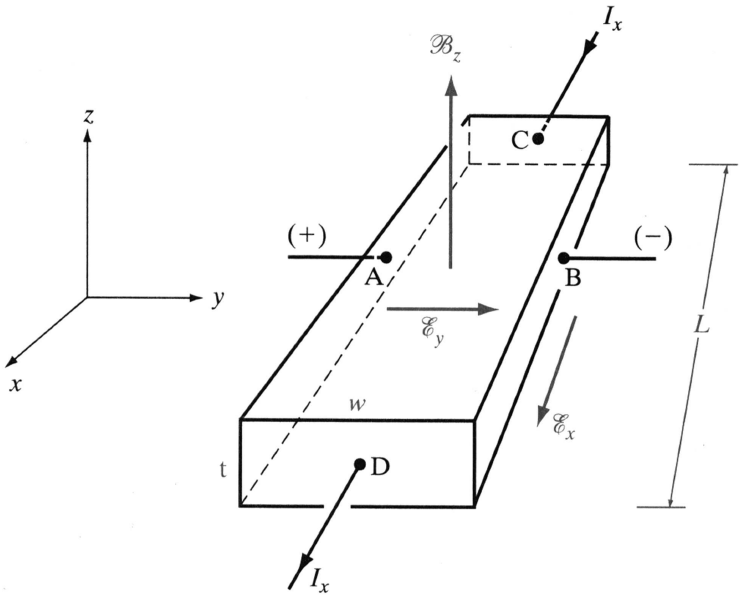

Figure 4.1: The Hall effect [10].

cause electric field E_y which continues to build until it exactly counters the deflection force of the magnetic field. E_y is known as the Hall field and $V_{AB} = E_y * w$ is known as the Hall voltage, which we can easily measure. We arrive at the solutions:

$$-v_x = \mu E_x \tag{4.5}$$

$$E_y = v_x B_z \tag{4.6}$$

where μ is the mobility. Using equation (4.3) the carrier concentration can be determined with a measurement of the current density [9].

The Hall effect is commonly used to measure the carrier concentration and mobility in semiconductors; several commercial setups for making the measurements are available.

4.1.1 N-type doping with Silicon

Silicon is commonly used as a n-type dopant in GaAs. Typical precursors are silane and disilane. Disilane is preferred because of its constant incorporation rate over the range of typical growth temperatures. By

Table 4.1: Doping of GaAs with disilane.

$\chi_{Si_2H_6}(\frac{mol}{min})$	$\chi_{Si_2H_6}/\chi_{TMGa}$	V/III ratio	Temperature (C)	n_e (cm^{-3})	μ_n ($\frac{cm^2}{Vs}$)
$2.23 * 10^{-7}$	$1.20 * 10^{-3}$	24	680	$4.83 * 10^{18}$	1310[1]
$5.58 * 10^{-8}$	$3.00 * 10^{-4}$	24	680	$2.09 * 10^{18}$	1680[1]
$2.23 * 10^{-8}$	$1.20 * 10^{-4}$	24	680	$9.58 * 10^{17}$	1970[1]
$8.93 * 10^{-9}$	$4.81 * 10^{-5}$	24	680	$9.70 * 10^{17}$	1710
$1.09 * 10^{-9}$	$5.87 * 10^{-6}$	24	680	$5.67 * 10^{16}$	4020

[1] These samples had poor symmetry factors, and thus likely have slightly higher mobilities

contrast, silane exhibits much higher incorporation at higher growth temperatures [11]. Disilane was chosen as the silicon precursor for the AIXTRON.

For doping characterization, 1 μm thick layers of GaAs were grown on top of a 50 nm thick layer of AlAs and an undoped GaAs buffer on semi-insulating (SI) substrates. Samples were cleaved into 10 mm squares and analyzed on a commercial Hall effect measurement system using Van der Pauw configuration [12]. Indium contacts were annealed and verified to be ohmic. Results are summarized in Table 4.1.

Silicon incorporation into GaAs is linear with molar flow ratio up to the saturation point. In GaAs, silicon incorporation saturates around $n_e = 5 * 10^{18}$ cm^{-3} [2]. Silicon doping results from this work exhibit this linear trend and saturate around the expected doping level. Doping data is plotted alongside data from literature in Figure 4.2.

At high doping levels, impurity scattering dominates in GaAs [9]. As a result, mobility decreases significantly with higher doping level in GaAs. Hall mobility data from Table 4.1 is plotted along with data from literature in Fig 4.3. The electron mobilities from this work are somewhat lower than they should be. This is most likely due to a particulate contamination issue in the disilane line that plagued the reactor for the first several growths. This set of samples all had significant visible defects from particle contamination in the layers. The problem has since been addressed and more recently grown material has been of better quality, and presumably higher mobility. There is a more detailed discussion of the contamination issue associated with the disilane line in Appendix D.

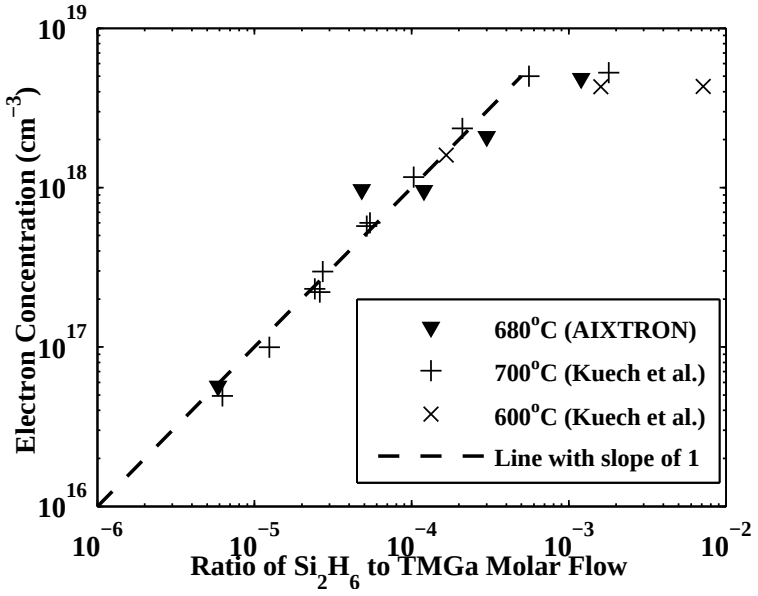

Figure 4.2: Electron concentration vs. molar flow ratio for silicon doping of GaAs [13].

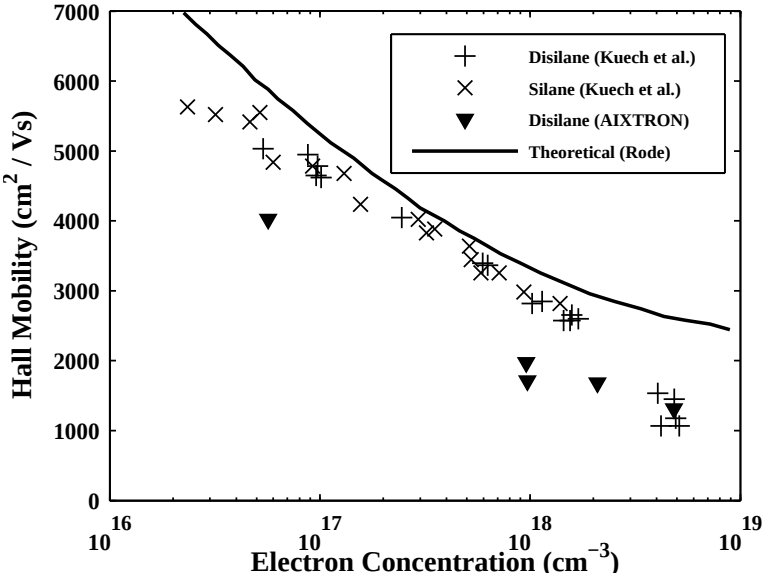

Figure 4.3: Electron mobility vs. electron concentration for silicon doping of GaAs [13].

Table 4.2: Doping of GaAs with carbon tetrabromide.

$\chi_{CBr_4}(\frac{mol}{min})$	$\chi_{CBr_4}/\chi_{AsH_3}$	V/III ratio	Temperature (C)	Anneal	n_h (cm^{-3})	μ_h ($\frac{cm^2}{Vs}$)
$2.07 * 10^{-6}$	$2.21 * 10^{-3}$	10	600	None	$1.18 * 10^{19}$	103
$2.07 * 10^{-6}$	$2.21 * 10^{-3}$	10	600	100 s @ 510° C[1]	$1.73 * 10^{19}$	87
$2.07 * 10^{-7}$	$2.21 * 10^{-4}$	10	600	100 s @ 510° C[1]	$2.25 * 10^{18}$	143
$2.07 * 10^{-7}$	$2.21 * 10^{-4}$	10	600	100 s @ 510° C[1]	$2.05 * 10^{18}$	153
$2.07 * 10^{-6}$	$2.21 * 10^{-3}$	10	600	100 s @ 510° C[2]	$1.91 * 10^{19}$	80

[1] In-situ anneal under hydrogen at 100 mbar
[2]Ex-situ RTP anneal under nitrogen at 1000 mbar

4.1.2 P-type doping with Carbon

Carbon can be used as a p-type dopant in GaAs. Carbon is preferable to group II dopants zinc, beryllium and magnesium due to its lower diffusion coefficient and higher free hole concentration [14]. Carbon doping can be either intrinsic or extrinsic. At low temperature and V-III ratio, the carbon from the pyrolyzed alkyl groups of metalorganic precursors incorporates into the material. In fact, this is why high growth temperatures and V-III ratio are used to grow n-doped material: to minimize compensation doping by the carbon from the alkyls. In intrinsic p-type doping we use this to our advantage. Extrinsic p-type doping is when a carbon precursor is used to allow p-type doping over a wider range of growth conditions. Carbon precursors include carbon tetrachloride (CCl_4) and carbon tetrabromide (CBr_4). CBr_4 was chosen as the carbon precursor for the AIXTRON.

For doping characterization, 1 μm thick layers of GaAs were grown on top of a 50 nm thick layer of AlAs and an undoped GaAs buffer on SI substrates. Samples were cleaved into 10 mm squares and analyzed on a commercial Hall effect measurement system using Van der Pauw configuration. Indium contacts were annealed and verified to be ohmic. Results are summarized in Table 4.2 and plotted in Figure 4.4.

When intrinsically doping with carbon, it commonly incorporates as a C-H radical. To activate the carbon, an anneal step is necessary. Even when extrinsically doping, carbon from the alkyl radicals is incorporated and thus an anneal can increase the doping level. Keiper et al. reported that SIMS analysis showed that a 100 s anneal at 510 °C was sufficient to fully activate all carbon. A doping increase of 1.5 to 2 times was observed after annealing [15]. Comparison of un-annealed and annealed samples from this work show similar doping enhancement factors of about 1.5. Mobilities of 65-80 $\frac{cm^2}{Vs}$ reported by Keiper et al. are well in agreement with the

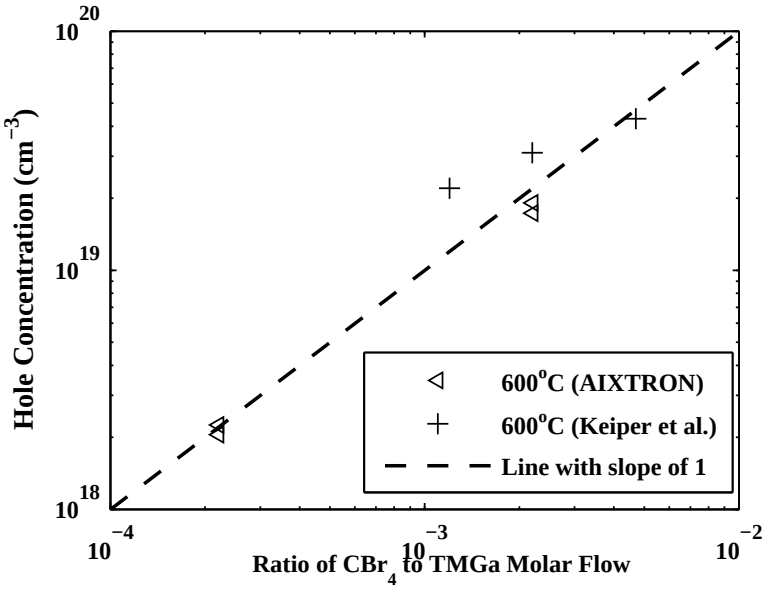

Figure 4.4: Hole concentration vs. molar flow ratio for carbon doping of GaAs [15].

mobilities of 80-87 $\frac{\text{cm}^2}{\text{Vs}}$ for doping above $1 * 10^{19}$(cm^{-3}).

4.2 X-Ray Diffraction

X-Ray diffraction (XRD) is an important technique in compound semiconductor analysis. To better understand diffraction, we consider the simple case of plane wave incidence. When a plane wave interacts with a material, spherical waves are scattered from the scattering centers. These spherical waves add constructively and destructively like any waves. In the case of a crystal lattice, the scattering centers are highly ordered and periodic, leading to some strong peaks at certain scattering angles, giving rise to the phenomenon of diffraction [16].

Bragg described crystal diffraction through his equation:

$$n\lambda = 2d \sin \Theta \tag{4.7}$$

Bragg considered each entire crystal plane as the scattering entity instead of each individual electron or nucleus. This simplification remains the most

Table 4.3: $Al_xGa_{1-x}As$ composition data from XRD.

$\chi_{\text{Group III}}(\frac{\text{mol}}{\text{min}})$	$\chi_{\text{TMAl}}/\chi_{\text{TMGa}}$	x	Growth Rate $(\frac{\text{nm}}{\text{s}})$
$1.85 * 10^{-4}$	.740	80%	2.3
$1.85 * 10^{-4}$	.498	60%	2.3
$1.86 * 10^{-4}$	.241	35%	2.3

useful description of crystal diffraction to this day [16].

Rocking curves from XRD can be analyzed to give information on the lattice constant and strain in a material layer. Analysis of the strain in a layer can be used to determine the composition percentage of ternary compounds. With a properly designed experimental structure, it is even possible to determine the thickness of layers. After XRD rocking curves are measured, software is used to simulate the expected results for the intended structure and compared to the experimental result. If the results are not in agreement, the values of layer thicknesses and compositions are iterated on until a simulation that is in good agreement with the experimental data is found.

XRD analysis for this work was performed on a Phillips X'Pert high resolution XRD system. The Cu-kα1 emission is selected through a 4-bounce monochromator. Rocking curves and simulation data for the analysis done in this work can be found in Appendix C.

4.2.1 Ternary Composition: $Al_xGa_{1-x}As$

To analyze $Al_xGa_{1-x}As$ composition a triple layer structure was grown. Each of the three layers was grown under a different precursor molar ratio with constant group III molar flow to equalize growth rate. The layers were separated by 50 nm AlAs barriers and a thin GaAs cap layer was grown to prevent oxidation. After a chromium stain etch, the layer thicknesses were examined by SEM to determine the growth rate. XRD on the sample gave the compositions of the three layers. Results are summarized in Table 4.3.

Table 4.4: $In_xGa_{1-x}As$ composition data from XRD analysis of superlattices grown at 625 °C.

$\chi_{\text{Group III}}(\frac{\text{mol}}{\text{min}})$	$\chi_{\text{TMIn}}/\chi_{\text{TMGa}}$	x
$1.00 * 10^{-4}$	.072	3.7%
$1.02 * 10^{-4}$	.150	7.7%
$1.02 * 10^{-4}$	.248	12.1%
$1.00 * 10^{-4}$	.360	16.6%
$1.01 * 10^{-4}$	.400	19.6%

4.2.2 Ternary Composition: $In_xGa_{1-x}As$

For $In_xGa_{1-x}As$ composition calibration, it is common to use a superlattice structure where layers of GaAs are alternated with the $In_xGa_{1-x}As$ for a number of periods so that layer thicknesses can be precisely determined in addition to the layer compositions. We cannot use this technique for $Al_xGa_{1-x}As$ because the lattice mismatch is so small that the fringe peaks are unresolvable even with high resolution equipment.

$In_xGa_{1-x}As$ / GaAs superlattices were grown at 625 °C. Superlattices varied from four to eight periods. More periods are desirable, but at higher indium compositions the number of periods and thicknesses of the layers must be limited to prevent strain relaxation. All superlattices were in good agreement with simulated data. The results of XRD on $In_xGa_{1-x}As$ superlattices are summarized in Table 4.4. Figure 4.5 plots indium composition against precursor molar flow ratio.

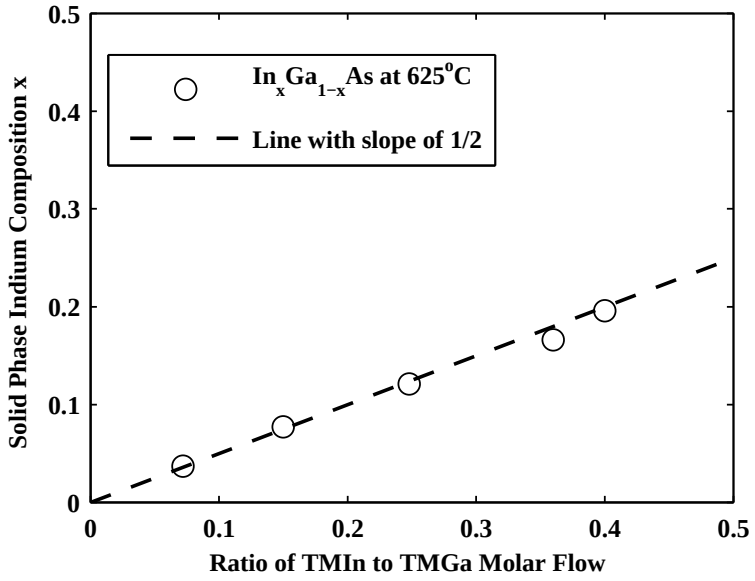

Figure 4.5: $\mathrm{In}_x\mathrm{Ga}_{1-x}\mathrm{As}$ composition (x) vs. precursor molar flow ratio.

CHAPTER 5

MATERIAL FOR RESEARCH

5.1 Quantum-Well Nanotubes

With the characterization data from the commissioning process, device structures may now be accurately grown. As a case study on the performance of the reactor, a series of strain-induced self-rolling semiconductor nanotube (SNT) structures were grown, processed, and analyzed. [1]

The SNT is a novel nanostructure formed by a strain-assisted rolling process first demonstrated by Prinz et al. [17]. To form a SNT, a three-layer epitaxial structure is grown where the top two layers are lattice-mismatched forming a strained bi-layer, and the bottom layer is made of a sacrificial material that may be selectively etched away. As the sacrificial layer is wet-etched away, the bi-layer is released from the epitaxial structure allowing the tensile strained half of the layer to contract and the compressively strained half of the layer to expand causing the bi-layer to curve and eventually roll over on itself forming a tube, as seen in Figure 5.1 [18]–[20].

The SNT process offers several distinct advantages over other methods of nanotube formation. The curvature of the released bi-layer is dependent on the overall and relative bi-layer thicknesses as well as the strain between the two films that form the bi-layer [21]; therefore the diameter of the tube can be designed to an arbitrary size by varying the composition and thicknesses of the epitaxial layers. Conventional lithography can be used to define the tube area before the undercut etch; therefore, the tube length, the number of times a tube rolls over on itself adding thickness to the wall,

[1] Nanotube structures were processed and analyzed by Ik Su Chun. Growth was done by the author.

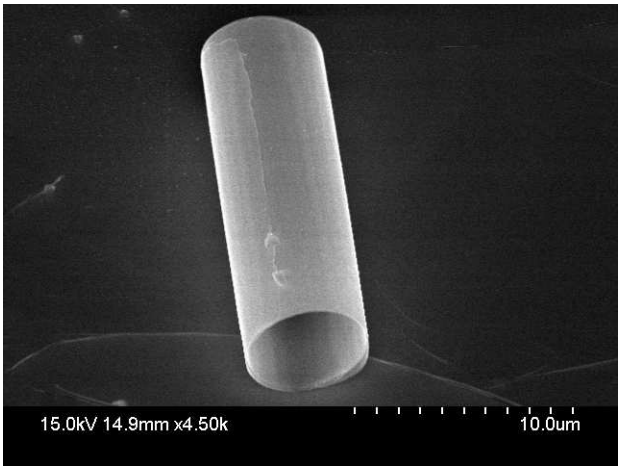

Figure 5.1: A semiconductor nanotube with an $In_{.15}Ga_{.85}As$ strained layer and an embedded 5 nm GaAs quantum well. The diameter is approximately 5.7 μm. (Image thanks to Ik Su Chun.)

and the precise location of the tube in an integrated structure can all be easily defined. Finally, by nature of the process, it is easy to integrate anything from quantum dots to entire devices with the inner wall of the tube by simply locating them on the surface of the epitaxial structure before it is rolled up.

The semiconductor nanotubes in this work have been designed with an embedded 5 nm thick GaAs quantum well. After fabrication, the nanotubes were collected and transferred to a silicon substrate for photoluminescence (PL) measurement. Figure 5.2 shows the collected nanotubes on the silicon substrate before PL measurement. PL data is plotted in Figure 5.3.

The diameters of the fabricated tubes were well in agreement with expected values, and the surface morphology was excellent. Strong photoluminescence proves that the material has high optical quality, and therefore has a low defect density. These facts show that the reactor performance is outstanding and that growth parameters are well understood.

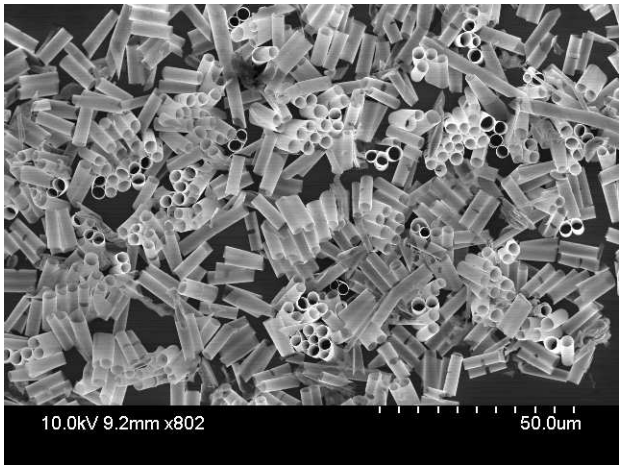

Figure 5.2: Semiconductor nanotubes with an $In_{.20}Ga_{.80}As$ strained layer and an embedded 5 nm GaAs quantum well after being transferred to a silicon substrate for PL. The diameters are approximately 4.5 μm. (Image thanks to Ik Su Chun.)

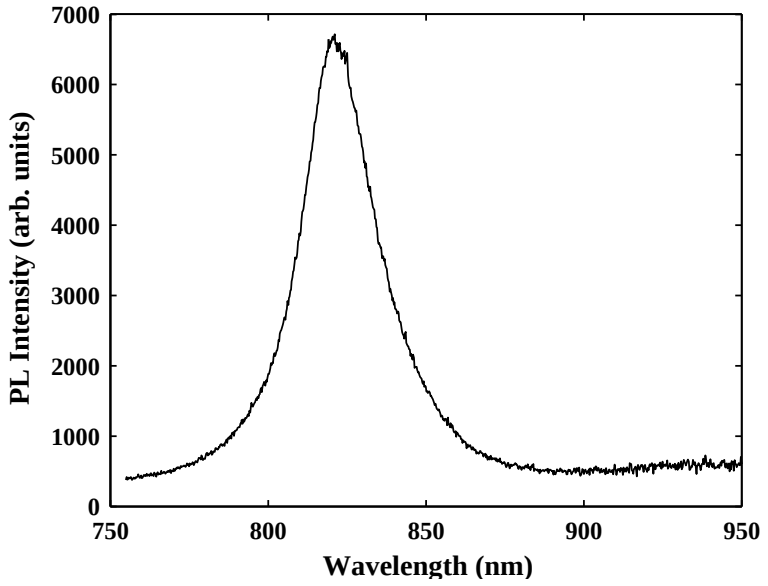

Figure 5.3: Photoluminescence data for semiconductor nanotubes with an $In_{.20}Ga_{.80}As$ strained layer and an embedded 5 nm GaAs quantum well. The background from the silicon substrate has been removed. (PL data thanks to Ik Su Chun.)

CHAPTER 6

MOVING FORWARD

Growth parameters for arsenide materials have been studied and calibrated for the AIXTRON reactor at MNTL. Material growth performance is quite good and the reactor is already growing research material.

Preparations to enable the use of a phosphine source are under way. Compared to arsine, the byproducts of flowing phosphine in the reactor present significant challenges in exhaust handling from the system. The byproduct of arsine pyrolysis, elemental arsenic, manifests itself in the exhaust system as black particulate dust which can be easily trapped by a woven filter element. The byproduct of phosphine pyrolysis, elemental phosphorous, manifests itself in one of three forms: white phosphorous, red phosphorous, or a mixture of both refered to as yellow phosphorous. White phosphorous is a waxy material that sticks to surfaces it comes in contact with. It is also highly toxic and spontaneously combustible. Red phosphorous is more stable than white phosphorous, yet is still highly flammible and toxic.

In contrast to the low-maintenance and simple-to-implement woven filter element needed to remove elemental arsenic from the exhaust stream, phosphorous is best condensed out of the exhaust stream using a cold trap. A cold trap requires a refrigeration system and coolant circulation system, significantly more compex than a particle filter. Furthermore, whereas a particle filter can capture elemental arsenic in the exhaust stream with almost 100% efficiency, a significant amount of white phosphorous can get past a cold trap during normal operation. As this phosphorous moves out of the system through the plumbing to the CDO furnace, it can condense onto the walls of the pipes, eventually leading to clogs. To reduce this effect, exhaust plumbing can be heated to around 100 °C, greatly reducing the potential for phosphorous to deposit on the walls. Plumbing in between the reactor exhaust outlet and the cold trap should also be heated.

Work is currently progressing on the installation of the heaters and cold trap necessary to use phosphine as a hydride source. Heater elements are protected with high temperature shut-off thermostats. The temperature of the exhaust plumbing is monitored at several locations to ensure adequate heating and to detect heater failures. A chiller and coolant circulation system have been acquired for use with the cold trap. Phosphine related elements of the exhaust handling system should be completely operational shortly. The phosphine toxic gas delivery system is presently ready to supply gas to the system.

After preparations and upgrades are finished to allow use of the phosphine source, work will begin on calibration of the phosphide material system. A full study of p and n type doping will be performed for the InP material system, as was done with the GaAs material system. HRXRD will be used to calibrate the compositions and thicknesses of strained layers. The new growth capabilities this reactor brings to MNTL will enable new research possibilities as well as supporting and enhancing established research projects.

APPENDIX A

AIXTRON AIX 200/4 S/N 1217 INITIALIZATION FILE

The initialization file for CACE, 1217.INI, had to be updated to reflect upgrades and changes to the system in order for all the hydride and metalorganic sources to function correctly. The updated version of 1217.INI is listed below.

```
;*********************************************************************
;*          1 2 1 7   C O N F I G U R A T I O N F I L E          *
;*********************************************************************
;*********************************************************************

[SYSTEM]
FIRST_ROB_ALERT=64
VERSION=1, 0, 2
VALVES=G, H, I, J, V, Z
FLOWCONTROLLER=F, X
PRESSURECONTROLLER=P
SOURCES=Q
SPECIALS=S
TEMPERATURES=T
CALCULATIONS=C
ALARM=A, K

[OS9HARDWARE]
UIC01=1
68K040=1
68K050=1
TSVME400=1
MPV904=4
MPV901=2

[ALARM]
;K1=57, 3, A1*A2*A3*A4*A5*A18*A19*A21
K1=0, 0,
K2=0, 0,
K3=0, 0,
K4=0, 0,
K5=0, 0,
K6=0, 0,
K7=0, 0,
K8=0, 0,
K9=0, 0,
K10=0, 0,
K11=0, 0,
K12=0, 0,
K13=0, 0,
K14=0, 0,
K15=0, 0,
K16=0, 0,
A1=3, SCRUBBER
A2=3, H2 MONITOR
A3=3, PROCESS STOP
A4=3, EXHAUST VENTILATION
A5=3, TOXIC GAS MONITOR
A17=3, REACTOR TEMPERATURE > LIMIT
```

```
A18=3, WATERLEAK
A19=3, PNEUMATIC
A20=3, HEATING SYSTEM
A21=3, H2 PRESSURE
A22=3, GAS SUPPLY
A23=3, REACTOR CABINET
A24=3, MFC ALERT
A25=3, COOLING WATER OFF
A26=3, MANUAL MODE
A27=3, dP OVER LIMIT
A28=3, REACTOR LEAK MONITOR
A29=3, EXCESS REACTOR TEMPERATURE
A30=3, EXCESS REACTOR PRESSURE
A31=3, N2 PRESSURE
A32=3, H2 PURIFIER

[SPECIALS]
S1=24, 0, 1, 1, Pump
S2=25, 0, 0, 1, Heater
S3=26, 0, 0, 1, Cooling
S4=27, 1, 0, 1, Control
S5=28,  0, 0, 1,  TVO
S10=57, 0, 1, 0,  ComputerEnable

[VALVES]
V1=0, 1, 0, 1, N2.line
V2=1, 0, 1, 1, H2.line
V3=2, 1, 0, 1, N2.run
V4=3, 0, 1, 1, H2.run
V5=4, 0, 0, 1, @
V6=5, 0, 0, 1, @
V7=6, 0, 0, 1, @
V8=7, 0, 0, 1, @
V9=8, 0, 0, 1, @
V10=9, 0, 0, 1, @
V11=10, 0, 0, 1, @
V12=11, 0, 0, 1, @
V13=12, 0, 0, 1, @
V14=13, 0, 0, 1, @
V15=14, 0, 0, 1, @
V16=15, 0, 0, 1, @
V17=16, 0, 0, 1, @
V18=17, 0, 0, 1, @
V19=18, 0, 0, 1, @
V20=19, 0, 0, 1, @
V21=20, 0, 0, 1, @
V22=21, 0, 0, 1, @
V23=22, 0, 0, 1, @
V24=23, 0, 0, 1, @
V25=32, 0, 0, 1, @
V26=33, 0, 0, 1, @
V27=34, 0, 0, 1, @
V28=35, 0, 0, 1, @
V29=36, 0, 0, 1, @
V30=37, 0, 0, 1, @
V31=38, 0, 1, 1, VentVac
V32=39, 0, 0, 1, PumpBypass
V33=40, 0, 1, 1, DOR
Z1=512, 0, 0, 0, HeatingControl
Z2=513, 0, 0, 0, HeatingManual

[FLOWCONTROLLER]
; wird ueber Dialog-Box eingetragen !! (ausser Name)
; Kanal , min , max , default,DA.min,DA.max,AD.min,AD.max, Name
F1=0,   0, 200.00, 20.00, 0, 32766, 0, 32766, @
F2=1,   0, 1000.0, 100.0, 0, 32766, 0, 32766, @
F3=2,   0,  500.0,  50.0, 0, 32766, 0, 32766, @
F4=3,   0, 1000.0, 100.0, 0, 32766, 0, 32766, @
F5=4,   0,  100.0,  10.0, 0, 32766, 0, 32766, @
F6=5,   0,  500.0,  50.0, 0, 32766, 0, 32766, @
F7=6,   0, 1000.0, 100.0, 0, 32766, 0, 32766, @
F8=7,   0,  500.0,  50.0, 0, 32766, 0, 32766, @
F9=8,   0,   50.0,   1.0, 0, 32766, 0, 32766, @
```

```
F10=9,  0, 1000.0,   1.0, 0, 32766, 0, 32766, @
F11=10, 0,   10.0,   2.0, 0, 32766, 0, 32766, @
F12=11, 0, 1000.0, 100.0, 0, 32766, 0, 32766, @
F13=12, 0,  200.0,  20.0, 0, 32766, 0, 32766, @
F14=13, 0, 1000.0, 100.0, 0, 32766, 0, 32766, @
F15=14, 0,  100.0,  10.0, 0, 32766, 0, 32766, @
F16=15, 0, 1000.0, 100.0, 0, 32766, 0, 32766, @
F17=16, 0,   50.0,   5.0, 0, 32766, 0, 32766, @
F18=17, 0, 1000.0, 100.0, 0, 32766, 0, 32766, @
F19=18, 0,  100.0,  10.0, 0, 32766, 0, 32766, @
F20=19, 0,   20.0,   2.0, 0, 32766, 0, 32766, @
F21=20, 0,   20.0,   2.0, 0, 32766, 0, 32766, @
F22=21, 0,  200.0,  20.0, 0, 32766, 0, 32766, @
F23=22, 0,   50.0,   5.0, 0, 32766, 0, 32766, @
F24=23, 0, 100.00,  10.0, 0, 32766, 0, 32766, @
F25=32, 0,  20.00,   2.0, 0, 32766, 0, 32766, @
F26=33, 0,   10.0,   2.0, 0, 32766, 0, 32766, @
F27=34, 0, 1000.0, 100.0, 0, 32766, 0, 32766, @
F28=35, 0, 10000.0, 500.0, 0, 32766, 0, 32766, RunMO
F29=36, 0, 5000.0, 250.0, 0, 32766, 0, 32766, RunHydrid
F30=37, 0,  500.0,  50.0, 0, 32766, 0, 32766, Rotation
F31=38, 0, 1000.0, 100.0, 0, 32766, 0, 32766, @
F32=39, 0, 1000.0, 100.0, 0, 32766, 0, 32766, @

[PRESSURECONTROLLER]
P1=24,   0.00, 2000.00, 1800.00, 0, 32766, 0, 32766, @
P2=25,   0.00, 2000.00, 1800.00, 0, 32766, 0, 32766, @
P3=26,   0.00, 2000.00,  500.00, 0, 32766, 0, 32766, @
P4=27,   0.00, 2000.00,  300.00, 0, 32766, 0, 32766, @
P5=28,   0.00, 2000.00, 1000.00, 0, 32766, 0, 32766, @
P6=29,   0.00, 2000.00, 1800.00, 0, 32766, 0, 32766, @
P7=30,   0.00, 2000.00, 1800.00, 0, 32766, 0, 32766, @
P8=31,   0.00, 2000.00, 1800.00, 0, 32766, 0, 32766, @
P9=56,   0.00, 2000.00, 1800.00, 0, 32766, 0, 32766, @
P10=57,  0.00, 2000.00, 1000.00, 0, 32766, 0, 32766, @
P11=58,  0.00, 1000.00,  990.00, 0, 32766, 0, 32766, ReactorPress

[TEMPERATURES]
T1=256, 0, 1000.0, 20.0, 0, 10000, 0, 10000, ReactorTemp
T2=257, 0,  100.0,  0.0, 0,  1000, 0,  1000, Power

[SOURCES]
;  SV,  RV1 ,RV2, SF , DF , Pr , IF1, PF1, IF2, PF2,Name
Q1=V5,   V17,   ,  F1,    ,    ,    ,  F2,    ,    , AsH3_1
Q2=V6,   V18,   ,  F3,    ,    ,    ,  F4,    ,    , PH3_1
Q3=V7,   V19,   ,  F6,  F7,  P2,  F8,    ,    ,    , Si2H6_1
Q4=V9,   V21,   , F11,    ,  P3,    , F12,    ,    , TMGa_1
Q5=V10,  V22,   , F13,    ,  P4,    , F14,    ,    , TMIn_1
Q6=V11,  V23,   , F15,    ,  P5,    , F16,    ,    , TMAl_1
Q7=V12,  V24,   , F17, F18,  P6, F19,    ,    ,    , CBr4_1
Q8=V13,  V26,   , F20, F24,  P7, F25,    ,    ,    , NONE_1
Q9=V14,  V27,   , F21, F22,  P8, F23,    ,    ,    , NONE_2
Q10=V16, V29,   , F26,    , P10,    , F27,    ,    , NONE_3
Q11=V30,    ,   , F31,    ,    ,    , F32,    ,    , LinerPurge

[CALCULATIONS]
C1=F29 + Q1 + Q2 + Q3
C2=F28 + Q4 + Q5 + Q6 + Q7 + Q8 + Q9 + Q10

[Materials]
TEAl=0, 0, 2361.200000, 8.999000, 73.820000, 114.000000
TMAl=0, 0, 2134.830000, 8.224000, 0.000000, 72.000000
TESb=0, 0, 2183.000000, 7.904000, 0.000000, 209.000000
TMSb=0, 0, 1697.000000, 7.706800, 0.000000, 166.860000
TBAs=0, 0, 1562.300000, 7.500000, 0.000000, 134.000000
TBP=0, 0, 3544.000000, 17.470000, 0.000000, 90.000000
DMCd=0, 0, 1850.000000, 7.764000, 0.000000, 142.880000
TMGa=0, 0, 1703.000000, 8.070000, 0.000000, 114.830000
TMIn=0, 0, 3014.000000, 10.520000, 0.000000, 159.930000
BCP2Fe=0, 0, 3680.000000, 10.270000, 0.000000, 186.040000
BCP2Mg=0, 1, 4198.000000, 25.140000, 0.000000, 154.300000
DESe=0, 0, 1924.000000, 7.905000, 0.000000, 137.000000
DETe=0, 0, 2093.000000, 7.990000, 0.000000, 185.720000
```

```
DEZn=0, 0, 2109.000000, 8.280000, 0.000000, 123.400000
DMZn=0, 0, 1560.000000, 7.802000, 0.000000, 95.450000
AsH3=1, 0, 0.000000, 0.000000, 0.000000, 78.000000
PH3=1, 0, 0.000000, 0.000000, 0.000000, 34.000000
SiH4=1, 0, 0.000000, 0.000000, 0.000000, 32.000000
H2S=1, 0, 0.000000, 0.000000, 0.000000, 34.000000
HCl=1, 0, 0.000000, 0.000000, 0.000000, 36.453000
Si2H6=1, 0, 0.000000, 0.000000, 0.000000, 62.170000
NONE=0, 0, 0.000000, 0.000000, 0.000000, 0.000000
CP2Fe=0, 0, 3680.000000, 10.270000, 0.000000, 186.040000

[DEVIATION]
F1=10.00,   60.00
F2=50.00,   60.00
F3=25.00,   60.00
F4=50.00,   60.00
F6=25.00,   60.00
F7=50.00,   60.00
F8=25.00,   60.00
F11=0.50,   60.00
F12=50.00,  60.00
F13=10.00,  60.00
F14=50.00,  60.00
F15=10.00,  60.00
F16=50.00,  60.00
F17=2.50,   60.00
F18=50.00,  60.00
F19=5.00,   60.00
F20=1.00,   60.00
F21=10.00,  60.00
F22=50.00,  60.00
F23=10.00,  60.00
F24=10.00,  60.00
F25=1.00,   60.00
F26=10.00,  60.00
F27=50.00,  60.00
F28=500.00, 60.00
F29=250.00, 60.00
F30=25.00,  60.00
F31=50.00,  60.00
F32=50.00,  60.00
P2=2000.00, 60.00
P3=2000.00, 60.00
P4=2000.00, 60.00
P5=2000.00, 60.00
P6=2000.00, 60.00
P7=2000.00, 60.00
P8=2000.00, 60.00
P10=2000.00,60.00
P11=1000.00,60.00

[OPTIONS]
F28=0001, 0, 10622904 0.00E+00 0.00E+00 0.00E+00 8.429996E-37, 10622904 4.00E+03 2.00E+06 5.00E+02 5.00E+02
P3=0001, 0, 598743 0.00E+00 0.00E+00 0.00E+00 8.429996E-37, 598743 4.00E+03 2.00E+06 5.00E+02 5.00E+02
P4=0001, 0, 10549472 0.00E+00 0.00E+00 0.00E+00 8.429996E-37, 10549472 2.40E+03 7.20E+05 3.00E+02 3.00E+02
P5=0001, 0, 598743 0.00E+00 0.00E+00 0.00E+00 8.429996E-37, 598743 8.00E+03 8.00E+06 1.00E+03 1.00E+03
P10=0001, 0, 1207 0.00E+00 0.00E+00 0.00E+00 8.429996E-37, 1207 8.00E+03 8.00E+06 1.00E+03 1.00E+03
F1=0001, 1, 597660 0.00E+00 0.00E+00 0.00E+00 8.429996E-37, 597660 1.60E+02 3.20E+03 2.00E+01 2.00E+01
F17=0001, 1, 10478337 0.00E+00 0.00E+00 0.00E+00 8.429996E-37, 10478337 4.00E+01 2.00E+02 5.00E+00 5.00E+00
F30=0001, 0, 10622904 0.00E+00 0.00E+00 0.00E+00 8.429996E-37, 10622904 4.00E+02 2.00E+04 5.00E+01 5.00E+01
F19=0001, 0, 10549459 0.00E+00 0.00E+00 0.00E+00 8.429996E-37, 10549459 8.00E+01 8.00E+02 1.00E+01 1.00E+01
P8=0001, 0, 10489864 0.00E+00 0.00E+00 0.00E+00 8.429996E-37, 10489864 1.440000E+04 2.592000E+07 1.80E+03 1.80E+03
Q1=0202, 37334, 218.998978, 0, 0.00, 100.00, 1.00, 62.892014, 0.00
Q2=0202, 5, 0.013350, 0, 0.00, 100.00, 1.00, 0.008795, 0.00
Q3=0202, 21097, 1.504073, 0, 0.00, 0.00, 1.00, 32.206234, 0.00
Q4=0202, 26429, 1.331064, 0, 0.00, -10.00, 1.00, 2.231960, 0.00
Q5=0202, 0, 0.00, 0, 0.00, 17.00, 1.00, 0.00, 0.00
Q6=0202, 23765, 2.225604, 0, 0.00, 17.00, 1.00, 21.025063, 0.00
Q9=0202, 846959, 17.539996, 0, 0.00, 17.00, 1.00, 417.626804, 0.00
S1=0000, 9227999, 0
V32=0000, 1594326, 0
V2=0000, 5109192, 0
F29=0001, 0, 10622904 0.00E+00 0.00E+00 0.00E+00 8.429996E-37, 10622904 2.00E+03 5.00E+05 2.500000E+02 2.500000E+02
```

```
V4=0000, 5102283, 0
V1=0000, 4887699, 0
V3=0000, 4889998, 0
C1=0001, 0.00, 10624046 0.00E+00 0.00E+00 0.00E+00 8.429996E-37, 1
C2=0001, 0.00, 10624046 0.00E+00 0.00E+00 0.00E+00 8.429996E-37, 1
S3=0000, 10556572, 0
S2=0000, 33531, 0
S4=0000, 102339, 0
T2=0001, 0, 10622904 0.00E+00 0.00E+00 0.00E+00 8.429996E-37, 10622904 0.00E+00 0.00E+00 0.00E+00 8.429996E-37
P11=0001, 0, 10622904 0.00E+00 0.00E+00 0.00E+00 8.429996E-37, 10622904 7.920000E+03 7.840800E+06 9.90E+02 9.90E+02
V33=0000, 2463413, 0
V22=0000, 2, 0
V17=0000, 39761, 0
V18=0000, 2, 0
V23=0000, 6755, 0
V24=0000, 1, 0
V27=0000, 1, 0
V29=0000, 2, 0
V31=0000, 1679608, 0
V19=0000, 5526, 0
V21=0000, 6346, 0
V5=0000, 40946, 0
F2=0001, 0, 597660 0.00E+00 0.00E+00 0.00E+00 8.429996E-37, 597660 8.00E+02 8.00E+04 1.00E+02 1.00E+02
V6=0000, 5, 0
F3=0001, 0, 10557839 0.00E+00 0.00E+00 0.00E+00 8.429996E-37, 10557839 4.00E+02 2.00E+04 5.00E+01 5.00E+01
F4=0001, 0, 10557839 0.00E+00 0.00E+00 0.00E+00 8.429996E-37, 10557839 8.00E+02 8.00E+04 1.00E+02 1.00E+02
V7=0000, 21104, 0
F6=0001, 0, 598743 0.00E+00 0.00E+00 0.00E+00 8.429996E-37, 598743 4.00E+02 2.00E+04 5.00E+01 5.00E+01
F7=0001, 0, 598743 0.00E+00 0.00E+00 0.00E+00 8.429996E-37, 598743 8.00E+02 8.00E+04 1.00E+02 1.00E+02
P2=0001, 0, 598743 0.00E+00 0.00E+00 0.00E+00 8.429996E-37, 598743 1.440000E+04 2.592000E+07 1.80E+03 1.80E+03
F8=0001, 0, 598743 0.00E+00 0.00E+00 0.00E+00 8.429996E-37, 598743 4.00E+02 2.00E+04 5.00E+01 5.00E+01
V30=0000, 41, 0
F31=0001, 0, 2712828 0.00E+00 0.00E+00 0.00E+00 8.429996E-37, 2712828 8.00E+02 8.00E+04 1.00E+02 1.00E+02
F32=0001, 0, 2712828 0.00E+00 0.00E+00 0.00E+00 8.429996E-37, 2712828 8.00E+02 8.00E+04 1.00E+02 1.00E+02
V9=0000, 26500, 0
F11=0001, 1, 598743 0.00E+00 0.00E+00 0.00E+00 8.429996E-37, 598743 1.600000E+01 3.200000E+01 2.00E+00 2.00E+00
F12=0001, 0, 598743 0.00E+00 0.00E+00 0.00E+00 8.429996E-37, 598743 8.00E+02 8.00E+04 1.00E+02 1.00E+02
V10=0000, 7, 0
F13=0001, 0, 10549472 0.00E+00 0.00E+00 0.00E+00 8.429996E-37, 10549472 1.60E+02 3.20E+03 2.00E+01 2.00E+01
F14=0001, 0, 10549472 0.00E+00 0.00E+00 0.00E+00 8.429996E-37, 10549472 8.00E+02 8.00E+04 1.00E+02 1.00E+02
V11=0000, 23832, 0
F15=0001, 0, 598743 0.00E+00 0.00E+00 0.00E+00 8.429996E-37, 598743 8.00E+01 8.00E+02 1.00E+01 1.00E+01
F16=0001, 0, 598743 0.00E+00 0.00E+00 0.00E+00 8.429996E-37, 598743 8.00E+02 8.00E+04 1.00E+02 1.00E+02
V12=0000, 4, 0
F18=0001, 0, 10549459 0.00E+00 0.00E+00 0.00E+00 8.429996E-37, 10549459 8.00E+02 8.00E+04 1.00E+02 1.00E+02
P6=0001, 0, 10549459 0.00E+00 0.00E+00 0.00E+00 8.429996E-37, 10549459 1.44E+04 2.592OE+07 1.80E+03 1.80E+03
V14=0000, 24, 0
F21=0001, 0, 10489864 0.00E+00 0.00E+00 0.00E+00 8.429996E-37, 10489864 1.60E+01 3.20E+01 2.00E+00 2.00E+00
F22=0001, 0, 10489864 0.00E+00 0.00E+00 0.00E+00 8.429996E-37, 10489864 1.60E+02 3.20E+03 2.00E+01 2.00E+01
V16=0000, 4137, 0
F26=0001, 0, 1207 0.00E+00 0.00E+00 0.00E+00 8.429996E-37, 1207 1.60E+01 3.20E+01 2.00E+00 2.00E+00
F27=0001, 0, 1207 0.00E+00 0.00E+00 0.00E+00 8.429996E-37, 1207 8.00E+02 8.00E+04 1.00E+02 1.00E+02
F23=0001, 0, 10489864 0.00E+00 0.00E+00 0.00E+00 8.429996E-37, 10489864 4.00E+01 2.00E+02 5.00E+00 5.00E+00
T1=0001, 0, 10622904 0.00E+00 0.00E+00 0.00E+00 8.429996E-37, 10622904 1.60E+02 3.20E+03 2.00E+01 2.00E+01
Z1=0000, 10622820, 0
Z2=0000, 961, 0
Q8=0202, 0, 0.00, 0, 0.00, -10.00, 1.00, 0.00, 0.00
F25=0001, 0, 10478326 6.237011E-315 6.419537E-315 0.00E+00 8.429998E-37, 10478326 1.60E+02 3.20E+03 2.00E+01 2.00E+01
F24=0001, 0, 10478326 6.277115E-315 6.540144E-315 0.00E+00 8.429998E-37, 10478326 8.00E+01 8.00E+02 1.00E+01 1.00E+01
V26=0000, 0, 0
V13=0000, 0, 0
F20=0001, 1, 10478326 6.155647E-315 6.326730E-315 0.00E+00 8.429998E-37, 10478326 1.60E+01 3.20E+01 2.00E+00 2.00E+00
P7=0001, 0, 10478326 6.498148E-315 6.922934E-315 0.00E+00 8.429998E-37, 10478326 1.440000E+04 2.592000E+07 1.80E+03 1.80E+03
V28=0000, 0, 0
V15=0000, 0, 0
Q7=0001, 0, 0.00, 0, 0.00, 0.00, 1.00, 0.00, 0.00
Q10=0001, 0, 0.00, 0, 0.00, 0.00, 1.00, 0.00, 0.00
Q11=0001, 0, 0.00, 0, 0.00, 0.00, 1.00, 0.00, 0.00
```

APPENDIX B

RECIPE TEMPLATE FOR AN EPITAXIAL GROWTH RUN

A recipe template has been written for system 1217. This template is intended to act as a starting point for new users to the system who are unfamiliar with the recipe syntax used on AIXTRON reactors. The template includes all the steps necessary to run a simple epitaxial growth from start to finish including: reactor initialization, temperature and pressure ramp phases, an oxide desorption step, growth of a GaAs buffer layer, and reactor cool down phase.

Recipe Template

```
#
#     Recipe Title
#
#     Description of recipe
#
#     Structure
#          1 um      etc.
#          100 nm    GaAs Buffer Layer
#                    SI GaAs Substrate
#

# In the initialization section be sure to setup all sources you need for your growth as
# well as remove any sources you don't need.  DO NOT change MO source pressures without
# first ramping them from their normal values.  Be sure to ramp them back to thier normal
# values when you are done!

#     MO "Normal" Pressures
#          TMGa_1       500 mbar
#          TMIn_1       300 mbar
#          TMAl_1       300 mbar
#          CBr4_1       500 mbar
#          DMZn_1       (Source not installed yet)

layer{
# Initialize system
30   N2.line close, H2.line open, N2.run close, H2.run open,     # Switch to Hydrogen
```

```
     RunMO = 5000, RunHydrid = 2000,
     LinerPurge.source = 500, LinerPurge.push = 500,
     Rotation = 50,
     AsH3_1.source = 100, AsH3_1.push = 400,                    # Arsine
     PH3_1.source = 200, PH3_1.source = 300,                    # Phosphine
     Si2H6_1.source = 50, Si2H6_1.dilute = 500,                 # Disilane
     Si2H6_1.press = 500, Si2H6_1.inject = 50,
     TMGa_1.source = 2.8, TMGa_1.press = 500, TMGa_1.push = 497, # Galium
     TMIn_1.source = 100, TMIn_1.press = 300, TMIn_1.push = 400, # Indium
     TMAl_1.source = 60, TMAl_1.press = 300, TMAl_1.push = 440,  # Aluminum
     CBr4_1.source = 50, CBr4_1.dilute = 500,                   # Carbon Tetra-bromide
     CBr4_1.press = 500, CBr4_1.inject = 50,
#    DMZn_1.source = 10, DMZn_1.press = 300, DMZn_1.push = 490,  # Zinc
     ReactorTemp = 750, ReactorPress = 1000,
     DOR open,    # Open DOR to evacuate for 30 seconds
     "Initialze System";

1    DOR close;    # Close DOR for reactor leak check

# Enable pressure control
     "Waiting for Pressure System", until ReactorPress >> 990;
5    "Enable Pressure Control", VentVac open, Control on;

# Pump down to process pressure (100 mbar)
2:00  ReactorPress to 100, "Pumping down";

# Set up injectors for low pressure
# Si2H6 especially has a tendency to stick closed at low flows
10   "Setting up dilute source injectors", Si2H6_1.inject = 100;
1    Si2H6_1.inject = 9;

# Enable heater
     "Enable Heater", Heater on, Cooling on, until ReactorTemp >> 150;

# Open lines for pre-purge
     AsH3_1.line open, until ReactorTemp >> 275;
1    AsH3_1.run open;

# Oxide desorption
      "Heating to Desorption Step", ReactorTemp = 750, until ReactorTemp >> 730;
10:00 "Oxide Desorption";

# Set growth temperature and pre-purge sources
5:00  "Set growth temp and pre-purge sources", ReactorTemp = 680,
      TMGa_1.line open, TMAl_1.line open, TMIn_1.line open;
      "Waiting for process temperature to be reached", until ReactorTemp == 680;

# Start growth
10    "Starting Growth Steps";

# GaAs buffer
1:00  "Growing Buffer", TMGa_1.run open;
5     "Buffer Done", TMGa_1.run close;
```

```
# Growth Layers Here

# Refer to CACE manual for syntax clarifications and advanced features like loops.

# Close lines
5     "Closing Lines", TMGa_1.line close, TMAl_1.line close, TMIn_1.line close;

# Start Cooling Down
5:00  "Cooling Down", Heater off;

# Fill reactor
5:00  ReactorPress to 1000, "Refill";

# Wait for 275 C
      "Cooling Down", until ReactorTemp << 275;
1     AsH3_1.run close, AsH3_1.line close;

# Wait for 100 C
      "Cooling Down", until ReactorTemp << 100;
5     "Standby", VentVac close, Control off;
}
```

APPENDIX C

HIGH RESOLUTION X-RAY DIFFRACTION ROCKING CURVES AND SIMULATION DATA

High resolution x-ray diffraction (HRXRD) was used to characterize $In_xGa_{1-x}As$ composition fractions and growth rates. Super-lattice structures, alternating layers of $In_xGa_{1-x}As$ and GaAs, were grown for several different $In_xGa_{1-x}As$ composition fractions. Super-lattices were designed to prevent strain relaxation, using four to seven periods of layer pairs and target $In_xGa_{1-x}As$ layer thicknesses of 4 nm or 8 nm. The results of the HRXRD work are plotted in Figures C.1 through C.5.

HRXRD was carried out in the Frederick Seitz Materials Research Laboratory Central Facilities, University of Illinois, which are partially supported by the U.S. Department of Energy under grants DE-FG02-07ER46453 and DE-FG02-07ER46471.

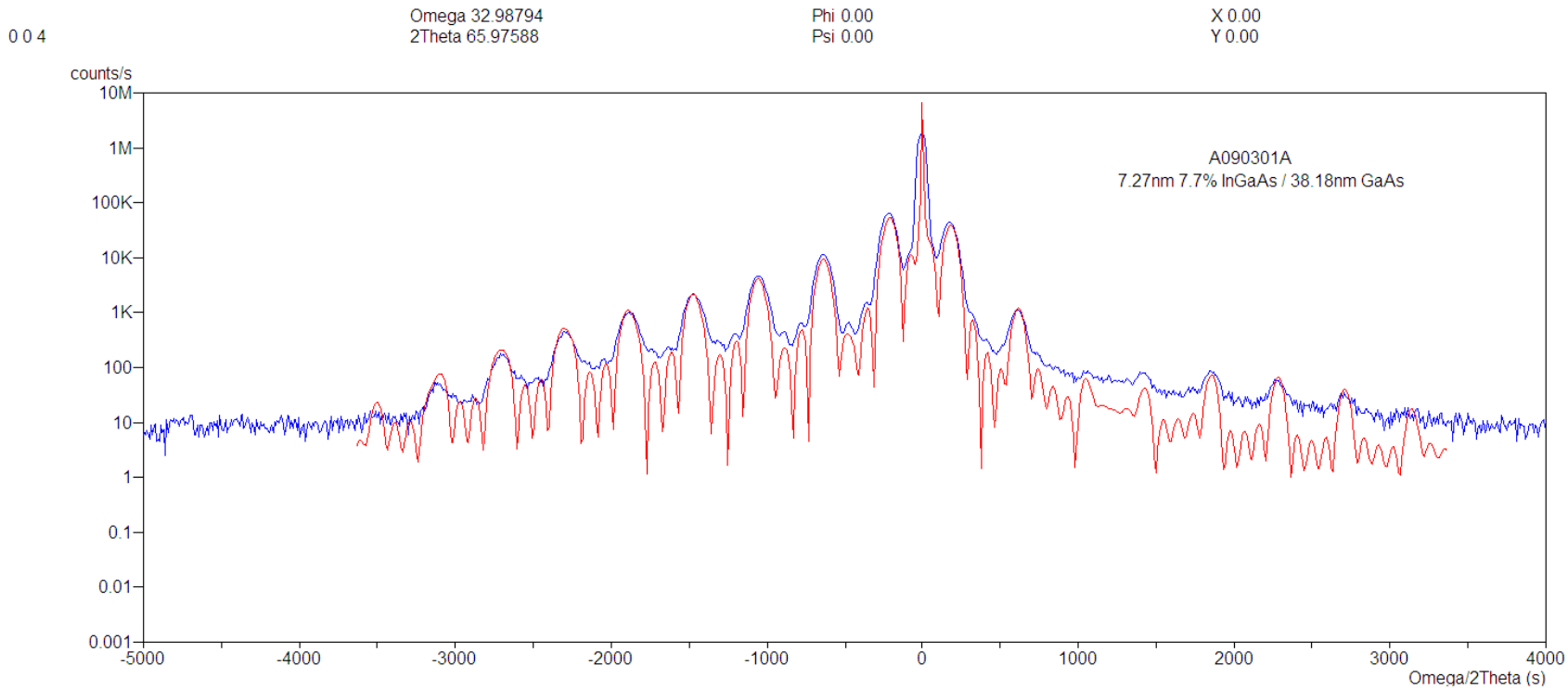

Figure C.1: HRXRD rocking curve and simulation results for an $In_xGa_{1-x}As$ / GaAs super-lattice, near GaAs [004]. Simulation and analysis showed this super-lattice had 7.3 nm, 7.7% In_xGaAs layers, and a period of 45.5 nm. This sample, serial number A090301A, was grown with four periods.

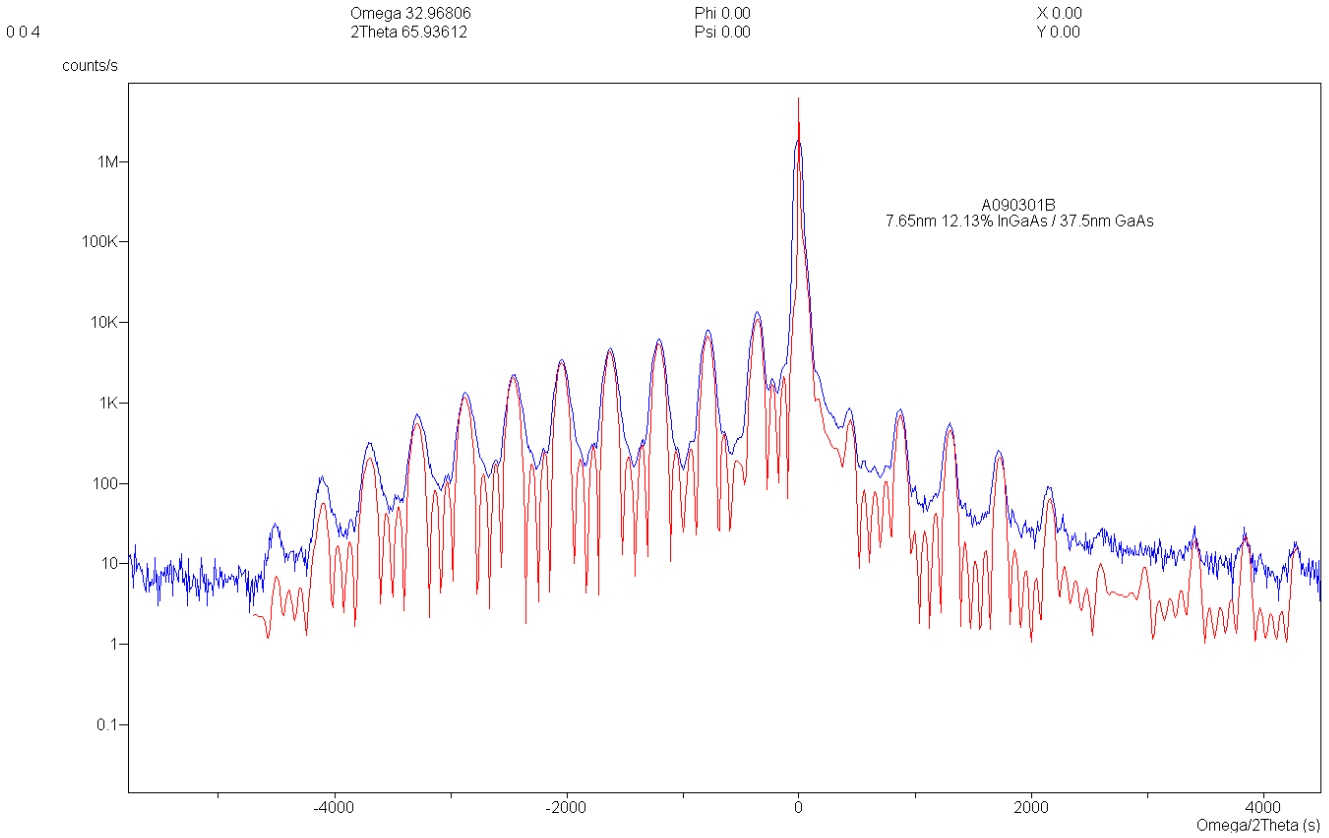

Figure C.2: HRXRD rocking curve and simulation results for an $In_xGa_{1-x}As$ / GaAs super-lattice, near GaAs [004]. Simulation and analysis showed this super-lattice had 7.7 nm, 12.1% In_xGaAs layers, and a period of 45.2 nm. This sample, serial number A090301B, was grown with four periods.

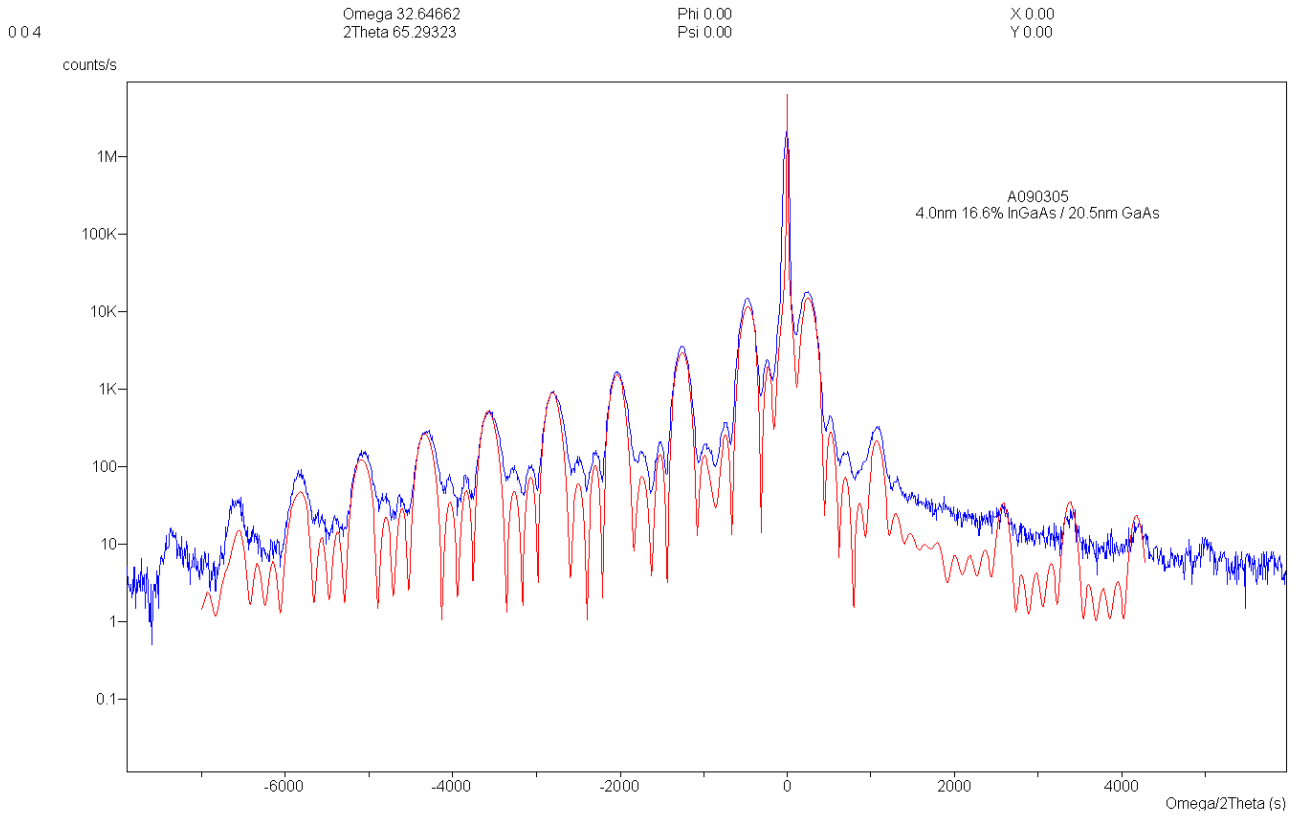

Figure C.3: HRXRD rocking curve and simulation results for an $In_xGa_{1-x}As$ / GaAs super-lattice, near GaAs [004]. Simulation and analysis showed this super-lattice had 4.0 nm, 16.6% In_xGaAs layers, and a period of 24.5 nm. This sample, serial number A090305, was grown with four periods.

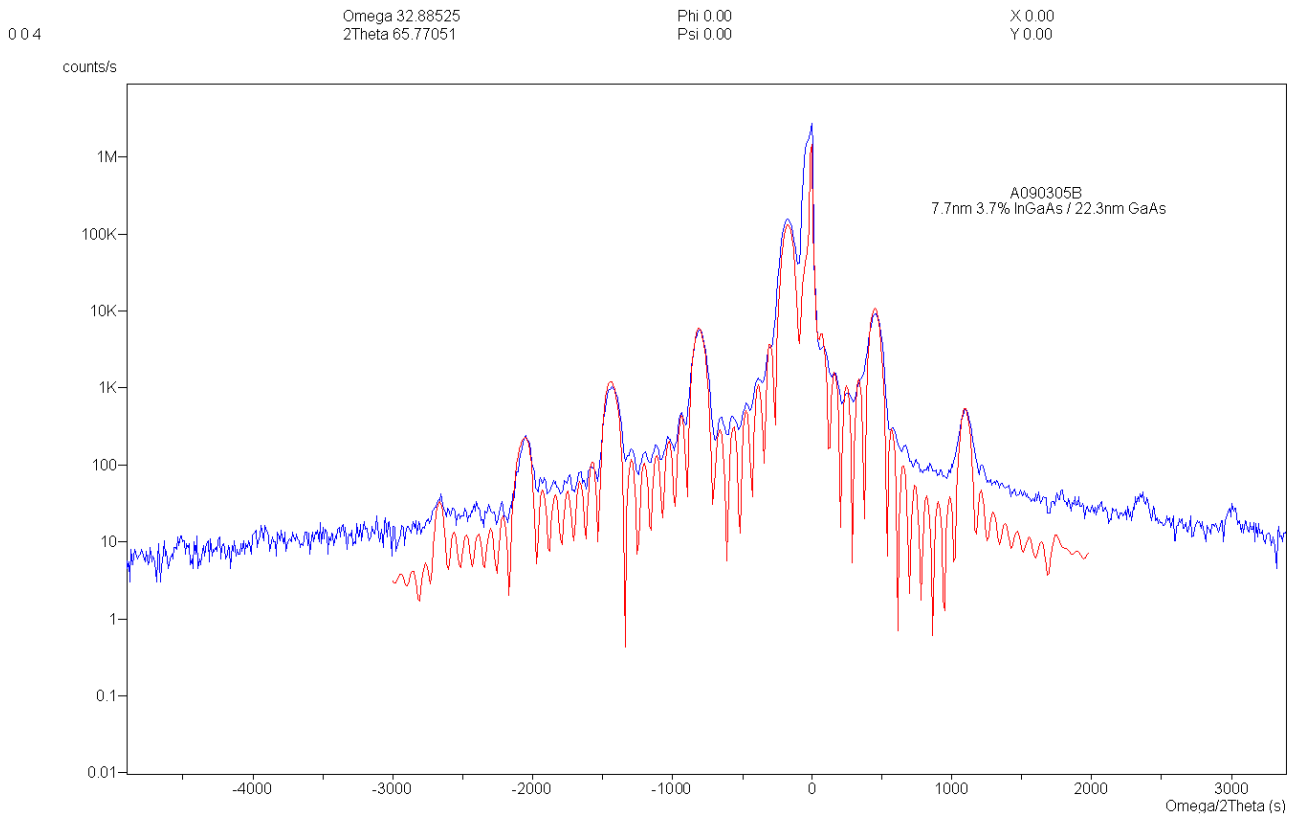

Figure C.4: HRXRD rocking curve and simulation results for an $In_xGa_{1-x}As$ / GaAs super-lattice, near GaAs [004]. Simulation and analysis showed this super-lattice had 7.7 nm, 3.7% In_xGaAs layers, and a period of 30 nm. This sample, serial number A090305B, was grown with seven periods.

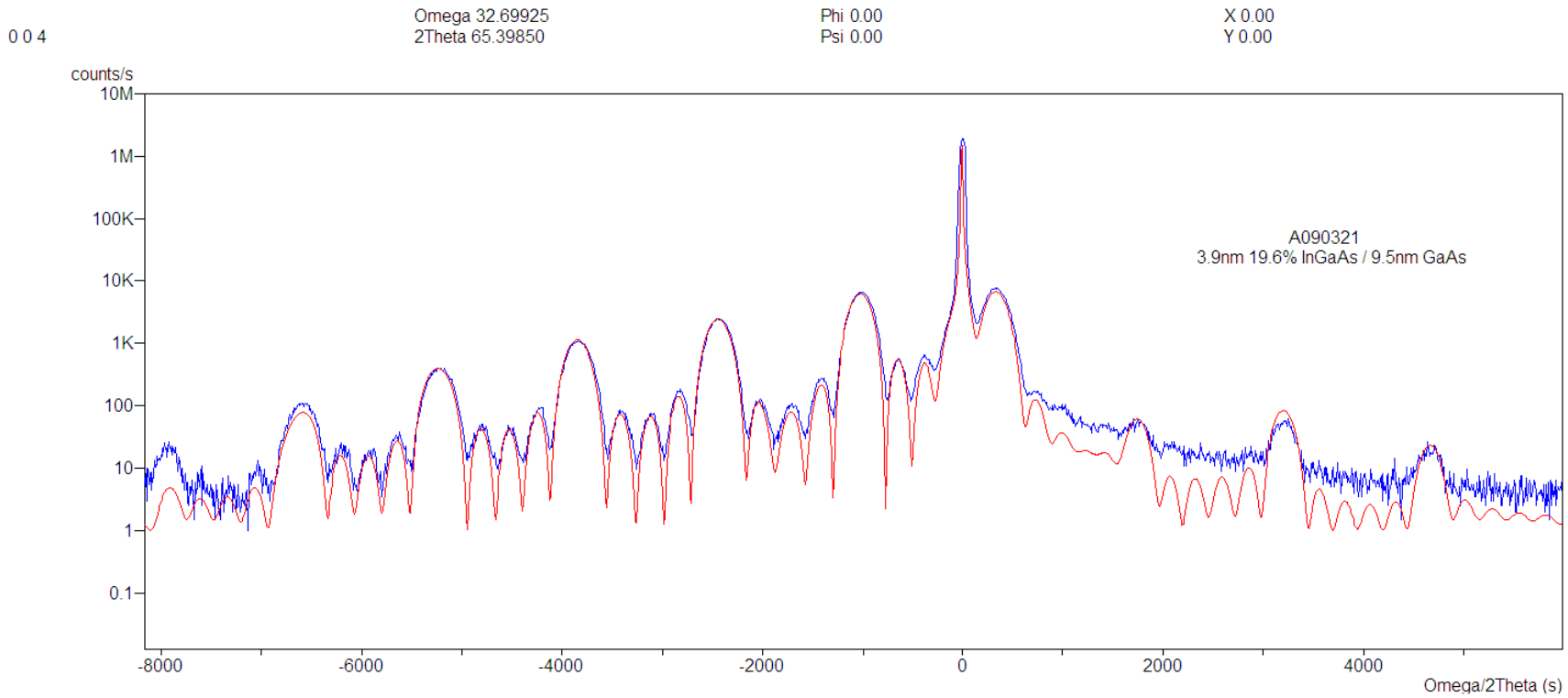

Figure C.5: HRXRD rocking curve and simulation results for an $In_xGa_{1-x}As$ / GaAs super-lattice, near GaAs [004]. Simulation and analysis showed this super-lattice had 3.9 nm, 19.6% In_xGaAs layers, and a period of 13.4 nm. This sample, serial number A0903021, was grown with five periods.

APPENDIX D

DISILANE LINE CONTAMINATION

The first growth attempted on system 1217 after its move to the University of Illinois was on November 25, 2008. The intended structure was 1 μm of silicon doped n-type 30% AlGaAs on 1 μm undoped AlAs on a 100 nm undoped GaAs buffer layer. A thin GaAs capping layer was also grown to prevent oxidation of the AlGaAs. The growth rates turned out to be faster than anticipated; the layers ended up 5.4 μm, 4.4 μm, and 440 nm respectively. More alarming, though, was the presence of a large quantity of dust in the n-type AlGaAs layer, leading to conical defects in the crystal that propagated upward toward the surface. SEM images of the dust and defects are shown in Figures D.1 and D.2. Note that the dust and defects only begin to appear after the uppermost layer begins to grow. Since the arsine, TMGa, and TMAl sources had all been introduced to the reactor at some point earlier in the growth and produced high quality material, it is presumable that the contaminant came from the disilane line.

The next growth was a repeat of the first structure, only without using disilane at any point. This growth yielded high quality material with no trace of the dust or defects observed in the first growth. In an attempt to remedy the situation, the disilane line was purged for 30 minutes at maximum flow. Subsequent material showed a much lower density of the suspect dust particles, although some dust was still present. A series of Hall effect samples were grown and a doping trend was established, but the mobility of the silicon doped n-type material was always below expectations from literature [13].

Several possible sources of this contamination have been identified. Disilane is pyrophoric, and creates small particles of silicon dioxide when it burns. An oxygen leak into the system is therefore a likely cause of dust contamination. However, extensive helium leak checking on the disliane line has failed to expose such a problem.

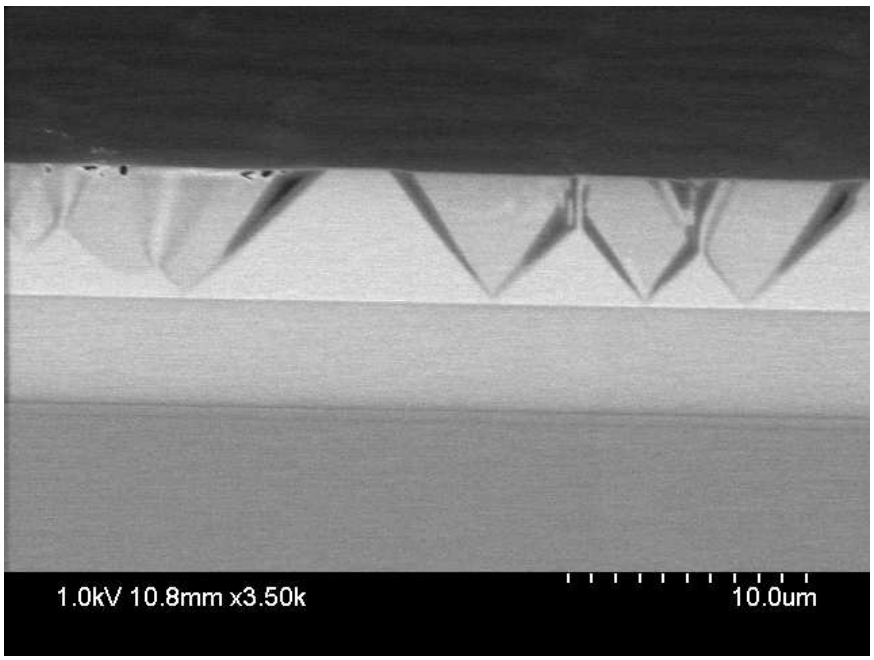

Figure D.1: Dust that deposited on the surface of the material during growth of the uppermost layer leads to a high density of conical defects in the crystal. Note that the dust distinctly appears only after the disilane source is introduced into the reactor for the final layer.

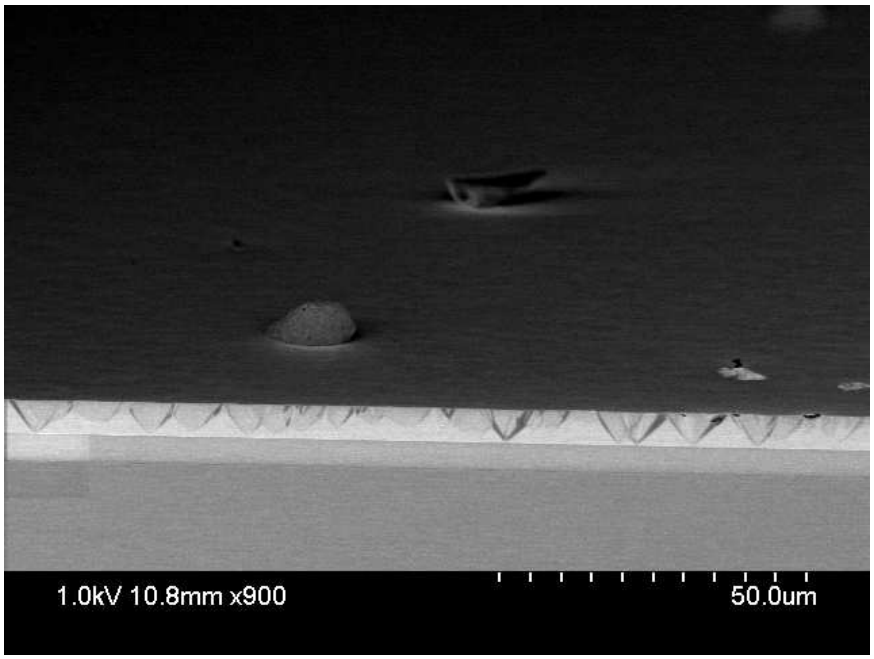

Figure D.2: Image of the dust and defects associated with introducing disilane into the reactor for the first time.

When the system was packaged for shipment to the University of Illinois, all open plumbing connections were to be capped. However, some of the caps were not tightened sufficiently and fell off during transport leaving some of the plumbing open to the environment. In addition, there was evidence that in transport the reactor jungle had been moved under a clearance that was too low for it to pass; there was a large dent in the ventilation duct which is the highest point of the system and drywall debris was present inside the cabinet. Several large pieces of broken drywall were found inside the cabinet and many MFCs were coated in a powdery substance that was presumably drywall dust. It was likely that significant quantities of drywall dust got into the open pipes, so a campaign to clean every pipe that could have possibly been exposed to the dust was undertaken before the first growth. A solution of 2:9 HF:HNO_3 was used followed by a DI rinse and methanol degrease. It is possible that this cleaning was not completely effective or a section of disilane related plumbing was missed completely.

Another possible source of the contamination in the disilane line is the toxic gas delivery cabinet. A former MNTL employee propped the door to the disilane cabinet open for a period of several years to prevent vibration that was occurring in the cabinet due to the ventilation air draw. When the author began to re-commission the cabinet for use with system 1217, all of its internal componenets were covered in a thick layer of dust and grease from the door being propped open. Despite the best efforts of the author to clean the internal components of the cabinet, it is possible that the source of the contamination in the reactor is dust in the cabinet itself. This scenario is highly unlikely, however, due to the presence of a high-quality particle filter upstream of the cabinet in the system itself that should filter any particles larger than 3 nm out of the disilane stream.

Through a number of experiments the dust contamination has presented itself in several different, yet similar ways. Figures D.3 through D.6 depict SEM images of the results of four experiments to learn more about the contamination issue. A brief summary of observations and implications is listed in Table D.1 on page 47. Energy dispersive X-ray spectroscopy (EDX) was used to try and determine the elemental composition of the dust particles. EDX was inconclusive as to the constituents of the particles beyond gallium, aluminum, and arsenic.

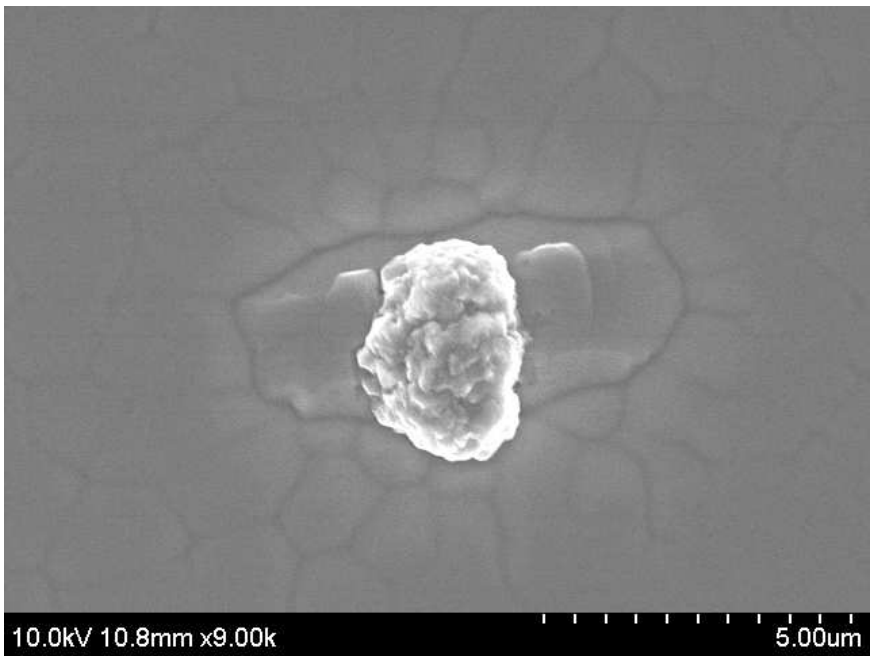

Figure D.3: SEM image of a dust particle and associated defect pattern in a 1 μm thick undoped 40% AlGaAs layer. Although the disilane source is not introduced into the reactor during this growth, these defects can be observed in decreasing density for several growths after the disilane line is used. The vast majority of defects on the sample are aligned with each other.

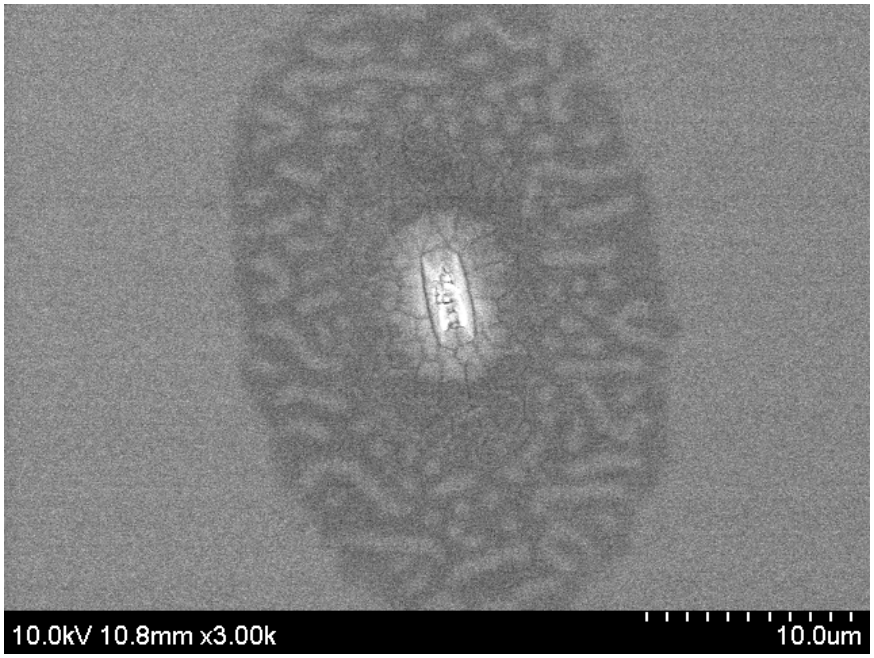

Figure D.4: SEM image of a dust particle and associated defect pattern in a 1 μm thick silicon-doped 40% AlGaAs layer. Disilane is introduced to the reactor during the growth of this layer, and experiments have shown that the density of defects observed is not proportional to the disilane flow. The vast majority of defects on the sample are aligned with each other.

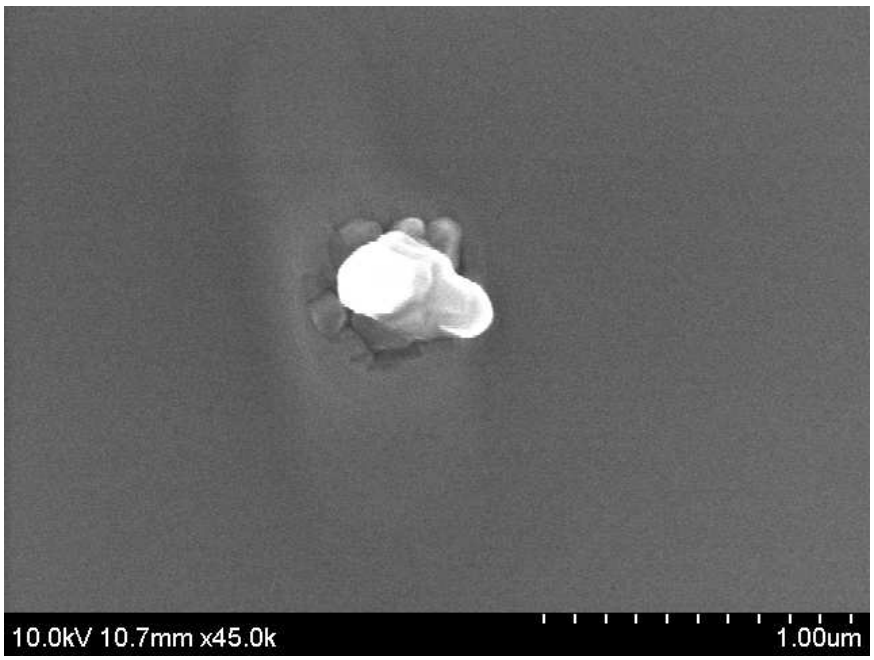

Figure D.5: SEM image of a dust particle and associated defect pattern in a 100 nm thick undoped 40% AlGaAs layer. Although the disilane source is not introduced into the reactor during this growth, these defects can be observed in decreasing density for several growths after the disilane line is used. Note the beginning of the formation of oval defects seen in the 1 μm thick layers.

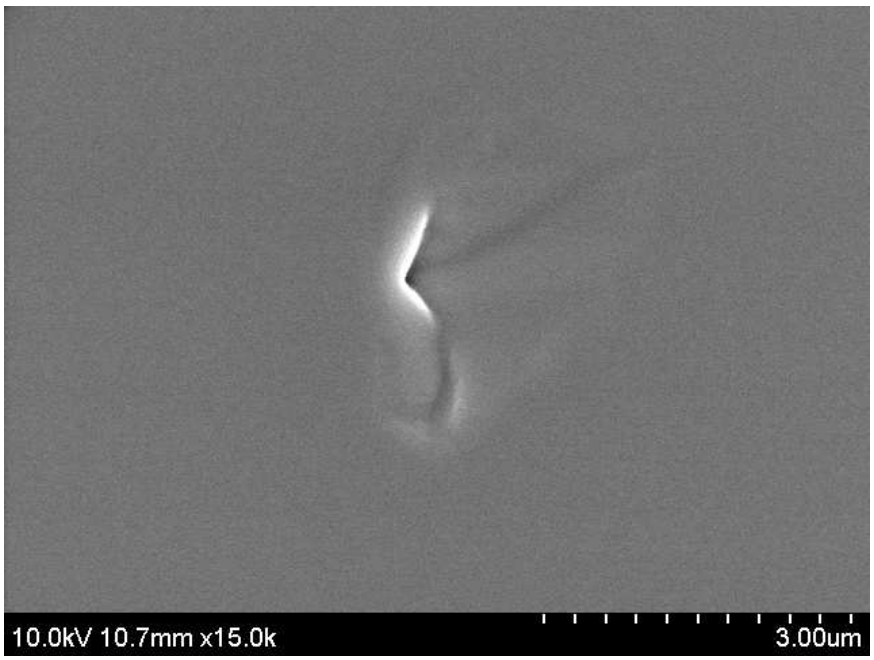

Figure D.6: SEM image of a dust particle and associated defect pattern in a 1 μm thick undoped GaAs layer. Although the disilane source is not introduced into the reactor during this growth, these defects can be observed in decreasing density for several growths after the disilane line is used. The vast majority of defects on the sample are aligned with each other.

Table D.1: Brief summary of some experimental observations made and implications inferred during disilane line contamination troubleshooting.

Observation	Hypothesis	Action taken	Conclusion	Comments
Large particles, conical defects present in Si-doped layer	Dust in toxic gas delivery line	30 minute purge of disilane line to vent	Significant improvement on next growth suggests dust in the line is the most likely source of contamination	Significant improvement after purge, but small dust particles continue to deposit in layer
Small particles continue to be present in significant quantities in the layers	Small particles and associated defects are causing observed low mobility in n-type material	Campaign to find and eliminate source of particles begun	No definitive conclusions at present time	Experimental details below
	Small dust may be from different source than large dust	Purge system for one week and run several consecutive growths without disilane	Small particle issue slowly got better and eventually disappeared by the fifth growth	Disilane, or the disilane plumbing (MFC, PC, pipes, etc.) must be involved in problem
Figure D.4	Control experiment to document particle issue initially observed	Normal growth with disilane	None, control only	Oblong defects due to particle deposition are aligned, may be crystal orientation dependant
Figure D.3	Disiliane itself may be involved in a detrimental reaction with another source or an oxygen leak into the system	Growth without disilane, but flowing hydrogen through disilane plumbing to run	Very similar defects show that disilane reaction is not likely a dominant factor	Experiment repeated many times with same result EDX analysis of particles inconclusive
Figure D.5	Growing a thinner layer may give us an understanding of how these defects nucleate	100 nm layer grown with no disilane, hydrogen through disilane plumbing	Defect nucleation appears to be directly caused by foreign particle deposition	EDX of particles to determine composition inconclusive
Figure D.6	TMAl may be involved in a detrimental reaction with a possible low level oxygen leak	Growth of GaAs attempted	Different defect nucleation observed, but underlying particles still grown into layer	TMAl may aggravate the problem, but doesn't appear to be the root cause

The latest effort to solve the disilane contamination issue has been to install a disilane chemical purifier in the system. This purifier will remove many common contaminants from the disilane stream, hopefully solving the problem for good.

APPENDIX E

SPC RUNS

Statistical process control runs are used to evaluate the performance of the system when problems are suspected, or after maintenance. Descriptions of SPC runs are listed in Table E.1.

Table E.1: SPC runs developed for use on system 1217.

Purpose	Name	Description	Characterization
Oxygen Background Check	ALGAASPL.EPI	1 μm n-doped 30% AlGaAs Layer, n = 3*10^{17}	Photoluminecsence should show a strong peak near 705 nm
Layer Interface Quality	INSL_8.EPI	Five Period $In_{.196}Ga_{.804}As$ / GaAs superlattice	HRXRD should show 3.9 nm InGaAs with a superlattice period of 13.4 nm and no relaxation.
Carbon Doping Check	CBR4_4.EPI	1 μm p-doped GaAs Layer, p = 2*10^{18}	Hall effect measurment should confirm expected doping level with a mobility around 150 $\frac{cm^2}{Vs}$
Silicon Doping Check	SI2H6_2.EPI	1 μm n-doped GaAs Layer, n = 2*10^{18}	Hall effect measurment should confirm expected doping level with a mobility around 2700 $\frac{cm^2}{Vs}$

REFERENCES

[1] A. G. Thompson, "MOCVD technology for semiconductors," *Materials Letters*, vol. 30, no. 4, pp. 255–263, Mar. 1997. [Online]. Available: http://www.sciencedirect.com/science/article/B6TX9-3SP6CW2-3C/2/b7b5064bdd2d109a9740bf0b4ef080c5

[2] G. B. Stringfellow, *Organometallic Vapor-Phase Epitaxy: Theory and Practice*, 2nd ed. San Diego: Academic Press, 1999.

[3] D. I. Fotiadis, S. Kieda, and K. F. Jensen, "Transport phenomena in vertical reactors for metalorganic vapor phase epitaxy : I. effects of heat transfer characteristics, reactor geometry, and operating conditions," *Journal of Crystal Growth*, vol. 102, no. 3, pp. 441–470, May 1990. [Online]. Available: http://www.sciencedirect.com/science/article/B6TJ6-46D6TXC-10Y/2/877851dfca808e6a1d4f19c3573e9e40

[4] D. V. Shenai-Khatkhate, R. J. Goyette, R. L. D. Jr., and G. Dripps, "Environment, health and safety issues for sources used in MOVPE growth of compound semiconductors," *Journal of Crystal Growth*, vol. 272, no. 1-4, pp. 816–821, Dec. 2004. [Online]. Available: http://www.sciencedirect.com/science/article/B6TJ6-4DHWWFR-H/2/c5404ef7e3f193ca4335a8db8a41bca4

[5] V. Fthenakis and B. Bowerman, "Environmental health and safety (EHS) issues in III-V solar cell manufacturing," in *Photovoltaic Energy Conversion, 2003. Proceedings of 3rd World Conference on*, vol. 1, 2003, pp. 681–684 Vol.1.

[6] V. E. Haven, "High pressure MOCVD reactor system," U.S. Patent 6066204, May 2000.

[7] *AIXTRON Operation & Technical Manual Projekt 1217*, AIXTRON Semiconductor Technologies GmbH, Aachen, Germany, 1992.

[8] *CACE 2 User Manual*, AIXTRON Semiconductor Technologies GmbH, Aachen, Germany, 1994.

[9] K. Hess, *Advanced Theory of Semiconductor Devices*. New York: IEEE Press, 2000.

[10] B. G. Streetman, *Solid State Electronic Devices*, 4th ed., ser. Prentice-Hall series in solid state physical electronics. Englewood Cliffs, N.J: Prentice Hall, 1995.

[11] T. F. Kuech, E. Veuhoff, and B. S. Meyerson, "Silicon doping of GaAs and AlxGa1-xAs using disilane in metalorganic chemical vapor deposition," *Journal of Crystal Growth*, vol. 68, no. 1, pp. 48–53, Sep. 1984. [Online]. Available: http://www.sciencedirect.com/science/article/B6TJ6-46DFRVJ-6W/2/f5bd261dfaf76830b40c1d9c2fd13710

[12] L. L. V. der Pauw, "A method of measuring specific resistivity and hall effect of discs of arbitrary shape," *Philips Research Reports*, vol. 13, no. 1, pp. 1–9, Feb. 1958.

[13] T. F. Kuech, B. S. Meyerson, and E. Veuhoff, "Disilane: A new silicon doping source in metalorganic chemical vapor deposition of GaAs," *Applied Physics Letters*, vol. 44, no. 10, pp. 986–988, May 1984. [Online]. Available: http://link.aip.org/link/?APL/44/986/1

[14] H. Li, F. Reinhardt, L. Birch, and G. Bradford, "High-efficient carbon-doped InGaAs/AlGaAs/GaAs quantum well lasers," *Journal of Crystal Growth*, vol. 263, no. 1-4, pp. 181–184, Mar. 2004. [Online]. Available: http://www.sciencedirect.com/science/article/B6TJ6-4BJ78NN-3/2/a2971e60f86f4af0caa2ae0dda35806a

[15] D. Keiper, "Comparison of carbon doping of InGaAs and GaAs by CBr4 using hydrogen or nitrogen as carrier gas in LP-MOVPE," *Journal of Crystal Growth*, vol. 197, pp. 25–30, Feb. 1999. [Online]. Available: http://adsabs.harvard.edu/abs/1999JCrGr.197...25K

[16] D. K. Bowen and B. K. Tanner, *High Resolution X-Ray Diffractometry and Topography*. London: Taylor & Francis, 1998.

[17] V. Y. Prinz, V. A. Seleznev, A. K. Gutakovsky, A. V. Chehovskiy, V. V. Preobrazhenskii, M. A. Putyato, and T. A. Gavrilova, "Free-standing and overgrown InGaAs/GaAs nanotubes, nanohelices and their arrays," *Physica E: Low-dimensional Systems and Nanostructures*, vol. 6, no. 1-4, pp. 828–831, Feb. 2000. [Online]. Available: http://www.sciencedirect.com/science/article/B6VMT-3YSY07V-70/2/64d79d338fd8344816bdc8c0d38d6b2a

[18] I. Chun, V. Verma, V. Elarde, S. Kim, J. Zuo, J. Coleman, and X. Li, "InGaAs/GaAs 3D architecture formation by strain-induced self-rolling

with lithographically defined rectangular stripe arrays," *Journal of Crystal Growth*, vol. 310, no. 7-9, pp. 2353–2358, Apr. 2008. [Online]. Available: http://www.sciencedirect.com/science/article/B6TJ6-4R53WMD-6/2/34e7e9f43289ef9cf126eb7af0f8fad7

[19] X. Li, "Strain induced semiconductor nanotubes: From formation process to device applications," *Journal of Physics D: Applied Physics*, vol. 41, no. 19, p. 193001, 2008. [Online]. Available: http://www.iop.org/EJ/abstract/0022-3727/41/19/193001

[20] I. S. Chun and X. Li, "Controlled assembly and dispersion of strain-induced InGaAs/GaAs nanotubes," *IEEE Transactions on Nanotechnology*, vol. 7, no. 4, pp. 493–495, 2008.

[21] P. O. Vaccaro, K. Kubota, and T. Aida, "Strain-driven self-positioning of micromachined structures," *Applied Physics Letters*, vol. 78, no. 19, pp. 2852–2854, May 2001. [Online]. Available: http://link.aip.org/link/?APL/78/2852/1